2016

Development of Folate Directed, Protein Based Photodynamic Therapy Agents

Rojenia Jones
Loyola University Chicago

LOYOLA UNIVERSITY CHICAGO

DEVELOPMENT OF FOLATE DIRECTED, PROTEIN BASED PHOTODYNAMIC THERAPY AGENTS

A DISSERTATION SUBMITTED TO

THE FACULTY OF THE GRADUATE SCHOOL

IN CANDIDACY FOR THE DEGREE OF

DOCTOR OF PHILOSOPHY

PROGRAM IN CHEMISTRY

BY

ROJENIA N. JONES

CHICAGO, ILLINOIS

AUGUST 2016

ACKNOWLEDGEMENTS

I would like to express my deepest appreciation to my advisor, Dr. Ken Olsen, who trusted and believed in me at times when I did not trust and believe in myself. His guidance, patience, and expertise created a space where mistakes were allowed and successes were celebrated. Working in his lab has taught me how to trust myself as a researcher and how to bring to life the ideas in my mind. During my tenure in his lab, he modeled consistency, kindness, and accessibility. For this I will be forever grateful and my prayer is that I will be able to pass the lessons learned to my future students.

I would also like to extend a huge thank you, to my committee members Dr. Crumrine, Dr. Dale, and Dr. Kanzok. Each of you have supersede all expectations that I had for a committee. I thank you for opening up your labs and sharing a considerable amount of time with me. I truly felt apart of each of your labs. Our conversations throughout the years were invaluable in completing this dissertation, and helped me navigate life as a graduate student. Thank you for taking an interest in my project in addition to taking an interest in me as a person and researcher.

In addition, I would like to thank Dr. Polack. Your help with designing and executing experiments with our lamp was an essential piece to completing this body of work.

Finally, I would like to thank my family and friends. Thank you to my parents, Wilson and Dionne Judkins, for always believing in me and instilling in me a work ethic that I am very proud of. Thank you to my "village" who along the way checked in and made sure that my personal and professional life was above average. Thank you to my children, Omer and Amber. Their innocence and pure curiosity in the world around them consistently reminded me why I wanted to become a scientist and taught me to appreciate the science in daily life. A very special thank you to my husband, Binyamin Jones. His love and support was present from the moment I decided to start my doctoral program and never faded. I thank him for the pep talks, hugs, and for always believing that I can be greater tomorrow than I am today; Iron sharpens iron.

To my Uncle, Roosevelt

TABLE OF CONTENTS

LIST OF TABLES

LIST OF FIGURES

CHAPTER ONE

INTRODUCTION

According to the World Health Organization (WHO) each year 8.2 million people die worldwide from cancer (World Health Organization, 2016). In the United States cancer is the second leading cause of death, and the American Cancer Society (ACS) estimates that one in two men and one in three women living in the U.S. will develop cancer at some point in their lives (American Cancer Society, 2016). Due to the prevalence of cancer there are countless institutions and scientist researching cures, treatments, and other areas of aid. The ACS has invested over $4 billion in research since 1946 (American Cancer Society, 2016). The National Cancer Institute, the U.S. government's primary agency for cancer related research, funded 3,100 institutions and over 14,000 investigators in 2014 (National Cancer Institute, 2016). Their efforts have assisted in lowering the death rate of cancer by 22% from 1990-2011 (National Cancer Institute, 2016). Although annual death rates are consistently decreasing, the projected number of new cases of cancer will increase by 70% over the next 20 years.

There are several options available for the treatment and management of cancer, some of which are: chemotherapy, radiation therapy, surgery, angiogenesis inhibitor therapy, and photodynamic therapy. Chemotherapy is the most popular course of treatment. Chemotherapy uses drugs to stop or slow the growth of cancer cells. It is often combined with radiation therapy of surgery. A major drawback of chemotherapy is its

robustness. It attacks both cancerous and healthy cells which leads to many unwanted side effects.

Radiation therapy damages cancer cells' DNA by using X-rays, gamma rays, or other charged particles. This method of treatment can damage healthy cells as well. Surgery is commonly coupled with radiation therapy to remove the tumor and some of the tissues around it, but there is high incidence of reoccurrence.

Angiogenesis inhibitor therapy prevents the formation of new blood vessels which in return prevents tumors from growing. This type of treatment does not "cure" the patient it only halts the tumors growth. To rid the patient of the cancer this therapy is combined with radiation and/or chemotherapy, leading to aforementioned unwanted side effects.

Photodynamic therapy (PDT) use light for the treatment of cancer (Figure 1). A light sensitive drug is given to a patient and absorbed by cells throughout the body. After a period of time most of the drug leaves the body, but the cancer cells retain the drug. The cells laden with the drug is exposed to light and the drug becomes toxic to cells destroying the cancer. One limitation of this method is the light needed to activate most drugs cannot pass through more than one centimeter of tissue (Vrouenraets, *et al.*, 2003) therefore this restricts the types and sizes of cancer treated. Also, the drug is absorbed by cells throughout the body and can be retained by non-cancerous cells which leads to unwanted cell death and prolonged light sensitivity throughout the entire body. For these reasons, our research focuses on the development of new PDT agents to increase specificity and to widen the scope of its use.

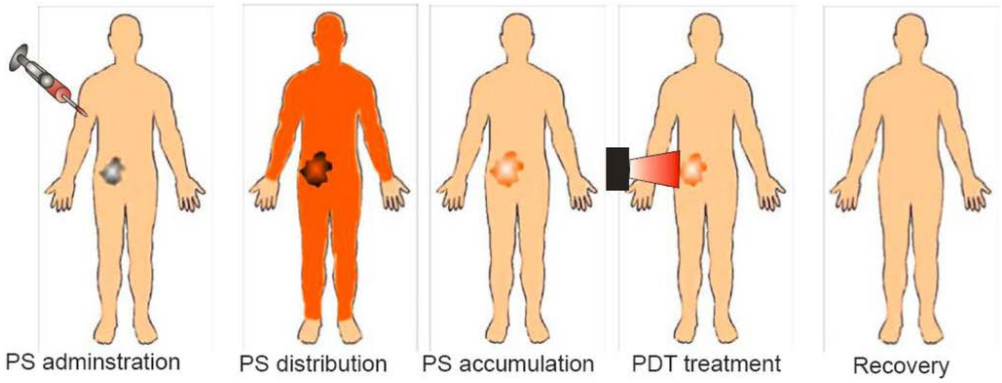

Figure 1. Photodynamic Therapy Schematic. A photosensitizer is given to the patient either topically or intravenously. Cancerous tumors preferentially retain the photosensitizer while healthy cells do not. The tumor is then irradiated with light at the appropriate wavelength which in turns activates the photosensitizer to become cytotoxic to the tumor. (Mroz, *et al.*, 2011)

Historical Perspective on Photodynamic Therapy

The use of phototherapy can be traced back to Ancient Egypt, Indian, and Chinese civilizations. In 1900 Oscar Raab observed that acridines (Table 1) in the presence of daylight are lethal to protozoan paramecium (Pervaiz and Malini, 2006). Raab along with his mentor, Herman Von Tappeiner, coined the term “photodynamic reaction” to differentiate their dynamic photobiological reactions that occurred in the presence of molecular oxygen from the photosensitization of photographic plates by certain chromophores (Pervaiz and Malini, 2006). In 1901 Niels Finsen discovered that red light can be used in the prevention of the formation and discharge of small pox pustules. He also discovered that ultraviolet light can be used to treat cutaneous tuberculosis (Dolman, *et al.*, 2003). He was awarded him the Nobel Prize in 1903 for this research (Dolman, *et al.*, 2003). In 1903 Tappeiner and Jodlbauer treated skin tumors with topically applied

eosin (Table 1) and white light (Dolman, *et al.*, 2003). This was the beginning of modern PDT.

Modern PDT began with the study of porphyrins as photosensitizers. In 1911 Hausmann studied hematoporphyrins (Table 1) to determine their photosensitivity and phototoxic effects (Pervaiz and Malini, 2006). In 1955 hematoporphyrin derivatives (HPD) were developed by Samuel Schwartz (Pervaiz and Malini, 2006). These derivatives were more phototoxic than hematoporphyrins (Pervaiz and Malini, 2006). Five years later Richard Lipson and Edward Baldes at the Mayo Clinic showed that Schwartz' HPD localized to tumors and emitted fluorescence which could be used to detect tumors (Pervaiz and Malini, 2006). Thomas Dougherty reported in 1975 that HPD and red light destroyed mammary tumor growth in mice and J.F. Kelly used HPD and light to kill bladder carcinoma in mice (Pervaiz and Malini, 2006). The first PDT drug was approved by the Federal Drug Administration (F.D.A.) in the U.S. in 1993.

Acridine	**Eosin**	**Hematoporphyrin**
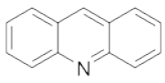	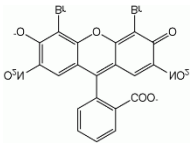	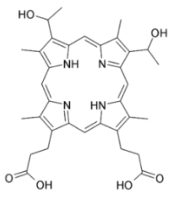

Table 1. Early Photosensitizers: Acridine and Eosin were observed in 1900 and 1903 respectively to be lethal in the presence of light. Hematoporphryins were used in 1911.

Photodynamic Therapy Mechanism

PDT has three requirements: a photosensitizer (PS), light at an appropriate wavelength, and molecular oxygen. A PS is a molecule that upon activation by light at a particular wavelength in the presence of molecular oxygen produces reactive oxygen species (ROS). The PS absorbs photons from light and this energy promotes one electron from the singlet state to a high energy orbital but it retains its spin. This state is short lived and is relaxed by fluorescence or internal conversion to heat (Robertson, 2009). This excited state may also undergo intersystem crossing in which the spin of the excited electrons inverts and forms an excited triplet state. This triplet state is long lived and can proceed via two routes, Type I reactions and Type II reactions (Figure 2) (Robertson, 2009). In Type I reactions the PS in the triplet state reacts directly with a substrate. The PS tranfers a proton and/or electron to the directly to the substrate to create a radical anion and/or cation respectively. These radicals then react with molecular oxygen to produce ROS (Robertson, 2009). In Type II reactions the PS in the excited triplet state reacts directly with molecular oxygen to produce singlet state oxygen (Robertson, 2009). Type I and II occur simultaneously and the ratio of the two is determined by the PS, concentration of substrate, availability of molecular oxygen, and various other factors. Hydroxyl radicals and singlet oxygen are both very reactive and have short half live (<0.04 μs), thus only molecules in close proximity to the ROS production site (<0.02 μm) are affected by PDT (Pervaiz and Malini, 2006).

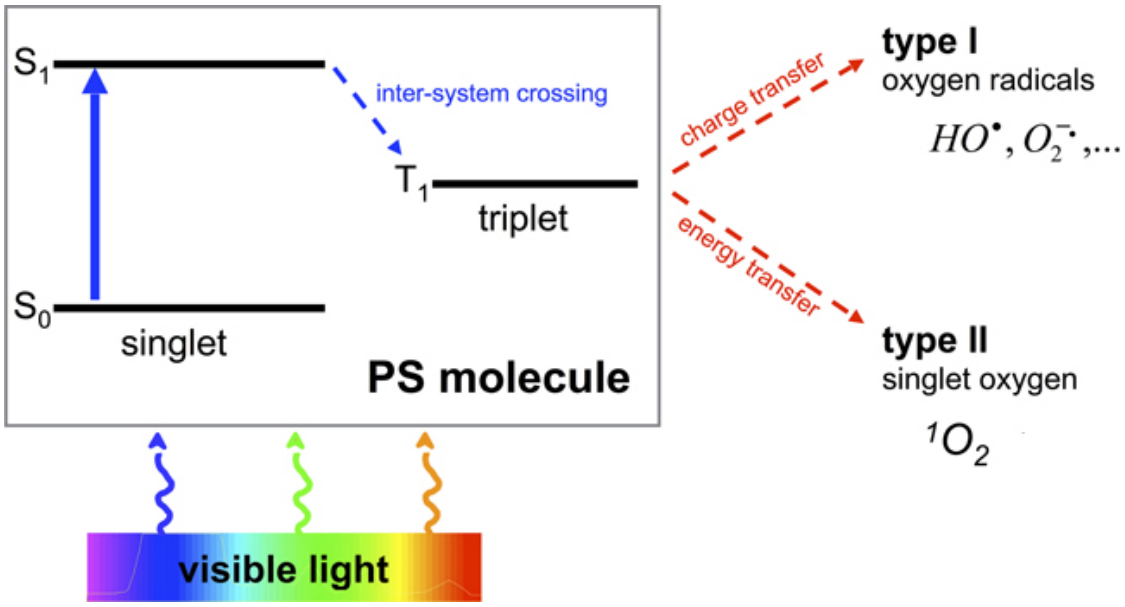

Figure 2. Type I vs. Type II reaction pathway. The PS absorbs photons from light and this energy promotes one electron from the singlet state to a high energy excited orbital. This excited state may undergo intersystem crossing in which the spin of the excited electrons inverts and forms an excited triplet state. This triplet state can proceed via two routes, Type I and II reactions. (Cieplik, *et al.*, 2014)

Modern Photosensitizers

An ideal photosensitizer will be chemically pure, chemically and physically stable, have a short time span between administration and accumulation in tumors, exhibit high selectively for cancerous cells, be retained preferentially by the cancerous cells, have minimal dark cytotoxicity, be cytotoxic only upon photoactivation, have a high quantum yield for the production of singlet oxygen, and be excreted from the body quickly (Pervaiz and Malini, 2006; Dolmans, *et al.*, 2003). Absorption between 600-800 nm has been deemed the optimal therapeutic window (Figure 3). Absorption and scattering of light by tissue increase as the wavelength decreases (Ethirajan, *et al.*, 2011;Pandey and Zheng, 2000). Nucleic acids and amino acids are present in tissue and

they absorb light between 250- 300 nm. Therefore, if a PS has a maximum absorbance over 600 nm these components will have very little effect on the PS effectiveness. Hemoglobin is the main component of tissues and is the biggest contributor to its absorption spectrum. Hemoglobin's absorptions peaks are all below 620 nm and those close to 620 nm are very weak. Melanin is also contained in tissues and has a broad absorption spectrum with strong absorption at shorter wavelengths (Ethirajan *et al.*, 2011,Franck and Nonn, 1995). Taking into account all of the components mentioned which absorb below 600 nm means that light penetration is minimal at wavelengths <600 nm. Wavelengths above than 800 nm do not provide enough energy to form a sizeable yield of ROS upon photoactivation (Ethirajan *et al.*, 2011; Agostinis *et al.*, 2011).

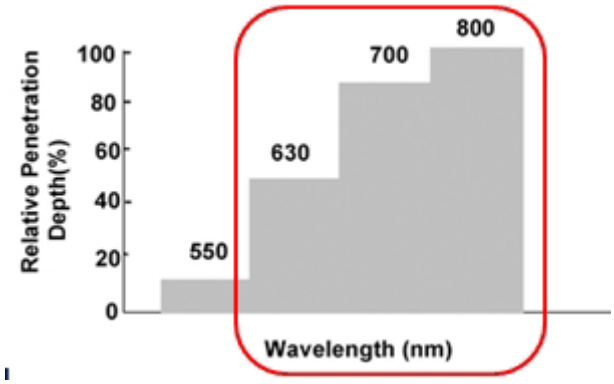

Figure 3. Optimal Therapeutic Window. Wavelength below 600nm are mainly absorbed by nucleic acids, amino acids, melanin, and hemoglobin. Wavelengths above 800 nm do not provide sufficient energy to generate appreciable amounts of singlet oxygen. (Ethirajan *et al.*, 2011; Seery, 2016)

First Generation Photosensitizers

Hematoporphyrins and HPD are referred to as first generation PS (Bonnet, 1999). HPD have a strong absorption band at 400 nm, commonly called the Soret band, and a four band absorption, Q band, which appears at 500, 540, 570, and 630 nm (Bonnet,

1999). Photofrin®, was the first porphyrin based PS used in clinical trials and subsequently the first to receive approval for use in the U.S. and Canada for the treatments of bladder, gastric, endobronchial, brain, and esophageal cancer (Dolman, *et al.*, 2003). Photofrin® consists of about 60 different porphyrins (Orenstein, *et al.*, 1996). Woodburn et al purified the porphyrins contained in Photofrin® and determined that porphyrins with cationic side chains localized in mitochondria and those with anionic side chains localized in lysosomes(Orenstein, *et al.*, 1996; Woodburn, *et al.*, 1991). Woodburn further investigated and determined that localization in mitochondria provided the most cellular death Orenstein, *et al.*, 1996; Woodburn, *et al.*, 1991;Woodburn, *et al.*, 1992).

These first generation PS were effective and made from readily available inexpensive reagents. Yet, HPD are complex mixtures that are difficult to reproduce, have modest activity, and poor selectively. In addition, first generation PS like Photofrin® have four to six week patient photosensitivity (Josefen and Boyle, 2008). Furthermore, the absorption at 630 nm, is very weak and outside of the optimum therapeutic window (Yamamto, *et al.*, 1999, Hirth and Michelsen, 1999). The weak absorption is compensated by using high doses of light of and drug which increases harmful side effects (Bonnet, 1999; Jori, 1992). These drawbacks lead to the creation of second generation PS. Many of these PS are porphyrin derivatives due to porphyrin's efficiency to generate singlet oxygen, lack of dark cytotoxicity, its ability to absorb light at longer wavelengths and have intense bands above 600 nm.

Second Generation Photosensitizers

Porphyrins. In order to capitalize on the advancements of Photofrin®, second generation PS began with attempts to produce pure porphyrins (Figure 4a). Many substituted porphyrins that have the lowest energy band red-shifted and/or intensified were synthesized. m-THPP (5,10,15,20-tetraakis(m-hydroxy-phenyl)porphyrin (Figure 4b) was determined to be 25-30 times more potent than HPD. Sulfonated derivatives of tetraphenylporphyrins (TPP) (Figure 4c) were synthesized, yet they appear to have some neurotoxicity in rats (Bonnet, 1999).

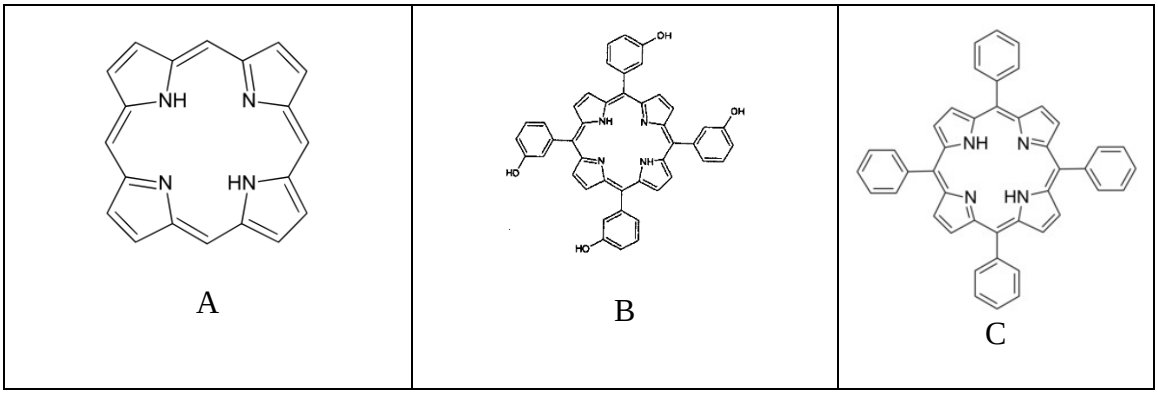

Figure 4. Chemical Structure of Porphyrins. (a) Porphyrin (b) m-THPP (c) TPP

Chlorins. Chlorins (Figure 5A) have strong absorption bands in the red region (Bonnet, 1999). They are derived from chlorophyll. They differ from porphyrin by the absence of at least one double bond in one of the pyrrole rings in the chlorin. Visudyne®, a benzoporphyrin derivative (BPD) (Figure 5b) is a chlorin synthesized from protoporphyrin that has absorption at 690 nm and it is rapidly accumulated in tumors which allow for irradiation on the same day that it is injected (Detty, *et al.*, 2006). Visudyne® has been approved for the treatment of wet age-related macular degeneration in the U.S. since 2000. It has a relatively short half-life with skin photosensitization

lasting less than a week. Foscan®, a synthetic chlorin, 5,10,15,20-tetraakis(m-hydroxy-phenyl)chlorin (m-THPC) (Figure 5c) is a potent photosensitizer that was approved in 2001 for use in Europe, Norway, and Iceland (Pervaiz and Malini, 2006). The U.S. Food and Drug Administration (FDA) rejected Foscan® in 2000 (Woodburn, *et al.*, 1992). Foscan® has a strong absorption peak at 652 nm, and drug and light dose are ten times lower than HPD. Foscan® is also 25-30 times more effective than HPD, but it lacks selectively, and has a six week skin photosensitization period which is a major drawback.

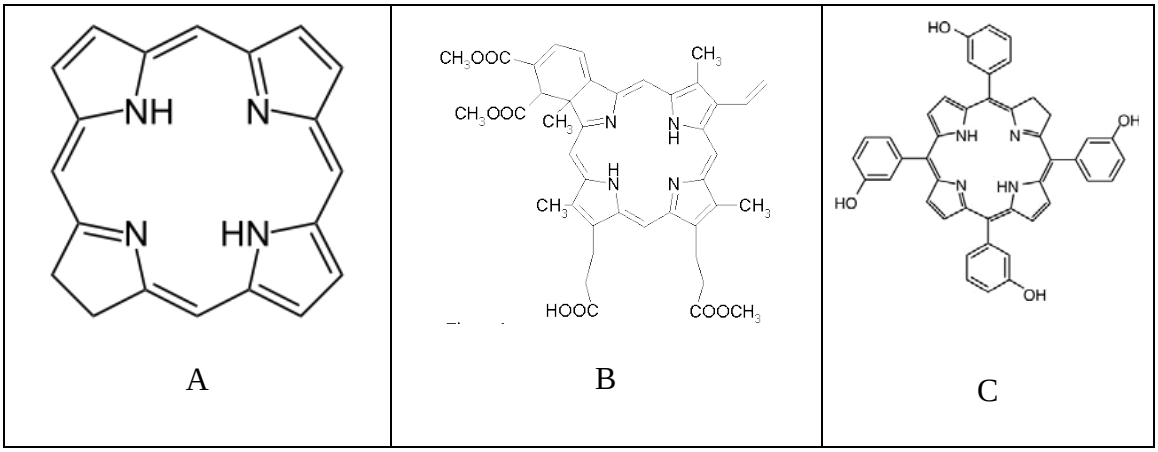

Figure 5. Chemical structures of Chlorins. (a) Chlorin (b)BPD (c)Foscan (m-THPC)

Phthalocyanines and related naphthalocyanines. Phthalocyanines (Figure 6b) and naphthalocyanines (Figure 6a) have macrocyclic π-system these compounds have strong absorption at 670 nm and 770 nm respectively. Due to their strong absorptions only a small dose is needed (Nyman and Hynninen, 2004; Bonnet, 1995). Phototoxicty increases when they are chelated with Zn^{3+} and Al^{3+}. These metals extend the lifetime of the triplet state (Orenstein, *et al.*, 1996). To increase hydrophilicity, sulfonated derivates were synthesized (Woodburn, *et al.*, 1992). Photosens®, a sulfonated aluminum phthalocyanine (Figure 6c), has been successfully used in clinical studies for the

treatment of cutaneous and endobronchial lesions and head/neck tumors (Uspenskii, *et al.*, 2000; Sokolov, *et al.*, 1995). Cellular uptake and phototoxicity are directly proportional to the degree of sulfonation (Woodburn, *et al.*, 1992). Unfortunately, sulfonation could not be controlled, and the product is a mixture of sulfonated phthalocyanines that could not be separated (Woodburn, *et al.*, 1992).

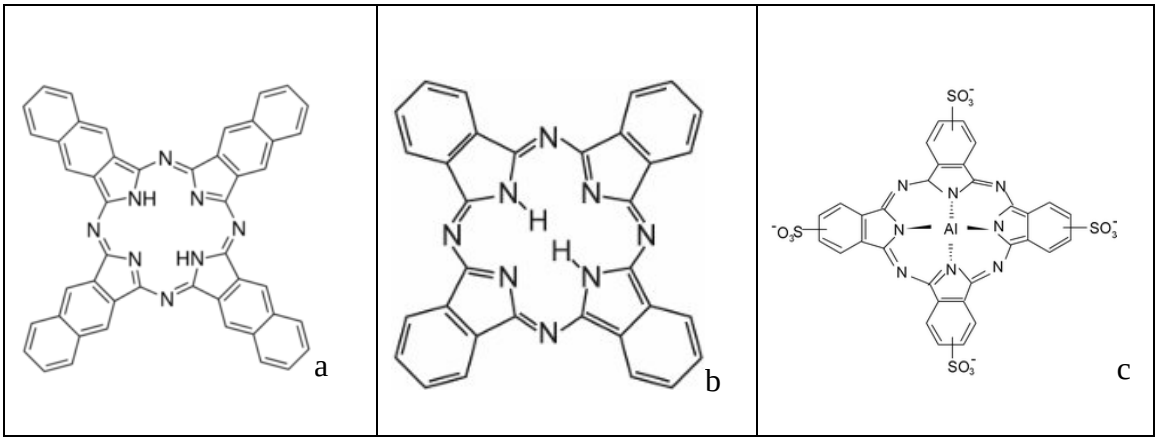

Figure 6. Chemical Structures of Phthalocyanines and Naphthalocyanines.
(a) naphthalocyanine (b)phyalocyanin (c) Photosens® ($AlPcS_4$).

d-Aminolevulinic acid (ALA). ALA (Figure 7a) is a naturally occurring amino acid, and an intermediate in the synthesis of heme. During the biosynthesis of the heme ALA is converted into proporphyrin IX (PpIX), which is phototoxic. PpIX (Figure 7b) accumulates in tumor with slight selectivity due to the activity of two different enzymes, ferrochelatase and porphobilinogen deaminase. Ferrochelatase is responsible for incorporating iron into PpIX, and porphobilinogen deaminase is responsible for forming uroporphyrin from porphobiligen (Woodburn, *et al.*, 1992). This provides for higher selectivity than Photofrin® but the maximum absorption is at 635 nm. Also, ALA is hydrophilic which makes it difficult penetrate cell membranes (Woodburn, *et al.*, 1992).

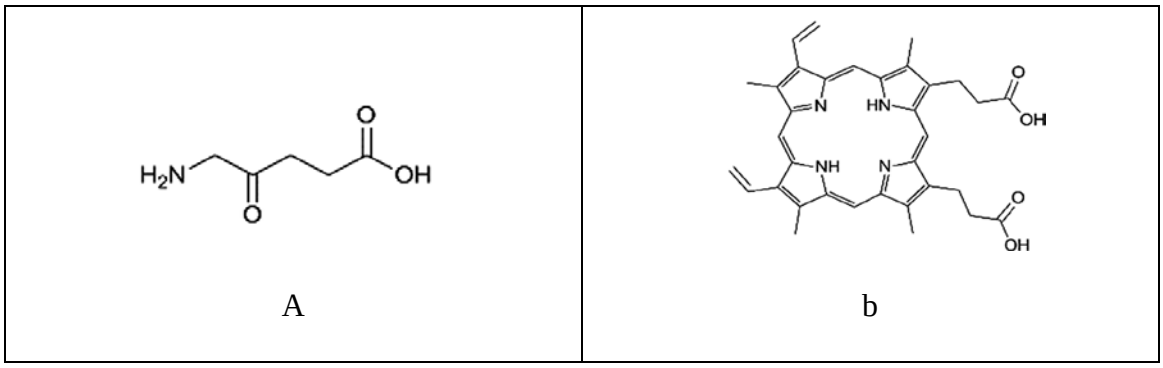

Figure 7. Chemical Structures of ALA and PpIX. (a)ALA (b)PpIX

Although first and second generation photosensitizers are beneficial in the treatment of cancers, they have one major disadvantage. They are not tumor selective. These photosensitizers accumulate in both normal and cancer cells which causes severe side effects. Therefore, a third generation of photosensitizers is currently being investigated. This new generation of compounds will maintain or enhance the characteristics of second generation PS, yet offer enhanced tumor selectivity.

Targeted PDT

A major problem with current cancer therapies is the low selectivity of the anti-cancer drug. Low selectivity of the drug allows for the toxic effects of the drug to exerted on both healthy and cancerous tissue. PDT can be considered to have increased selectivity over traditional cancer therapies because the toxic effects of the drug in only induced by light, and the tissues not exposed to light will be spared the toxic effects. Yet, some tissues that are exposed to environmental light after administering PS can exhibit some phototoxicity that persists for several weeks after treatment. Therefore, targeted PDT is the focus of the third generation PS. By covalently or non-covalently attaching a targeting moiety to the PS specificity is increased. Such approaches have included the use

of low density lipoproteins (LDL) conjugates, monoclonal antibodies conjugates, transferrin conjugates, and macrophage scavenger receptor mediated protein conjugates. Conjugates of PS to small molecules such as steroids, and sugars to nanoparticles have been investigated to improve cell-type specificity in targeted PDT.

Liposomes and low density lipoproteins. Liposomes prepared with the ethoxy castor oil, Cremphor-EL, has been used for the delivery of hydrophobic PS (Reddi, 1997). It was shown that 70-80% of hematoporphyrin that was administered in dipalmitoylphosphatidylcholine (DPPC) liposomes became associated with lipoproteins, while 10% of hematoporphyrin was associated with protein fraction after delivery in phosphate buffered saline (Reddi, 1997). These studied indicated that the liposomal hematoporphryin accumulated in the tumor at a slower rate than the free drug, but it reached a maximum tumor concentration twice as high. Importantly, the skin concentration was lower than the free drug (Reddi, 1997).

Proliferating tumor cells and tumor microvascular endothelial cells overexpress LDL receptors. Thus, LDL conjugates can be used as targeting vehicles to enhance a PS intracellular accumulation and potentially its photodynamic activity via receptor mediated endocytosis pathway (Sharman, *et al.*, 2004). LDLs also play an important role in the transport of hydrophobic PS across the plasma membrane (Reddi, 1997). The binding of serum proteins to the PS is mainly controlled by the hydrophilicity of the PS (Reddi, 1997). Moderately hydrophobic PS have been shown to be transported in the bloodstream by albumin, whilst highly hydrophobic are transported by lipoproteins. In human erythrocytes, phthalocyanine-loaded LDL conjugates have been shown to induce

cytotoxic effects by targeting specific thiol groups at the cell membrane (Martins, *et al.*, 2002). The efficiency and selectivity of PS delivery to LDL receptors in cancer cells depends on the conformational change of the LDL structure. The hydrophobic Zn(III)-phthalocyanine (ZnPc) PS bound to human LDL (ZnPc-LDL) exhibits low affinity for LDL receptors and the conjugate was internalized into human HT1080 fibroblasts through non-specific endocytosis. The lack of affinity was due to changes in the apolipoprotein-B structure induced by phthalocyanine association in the ZnPc-LDL conjugate (Polo, *et al.*, 2002). To improve the incorporation of phthalocyanine-LDL complexes, an attempt has been made to introduce a 12 carbon alkyl chain to aluminum tetrasulfonated phthalocyanine ($AlPcS_4$) through a sulfonamide bond (Urizzi, *et al.*, 2000). This conjugate showed tumor regression activity and was effective against A549 adenocarcinoma lung cancer cells (Sharman, *et al.*, 2004; Urizzi, *et al.*, 2000).

To enhance selectivity PS-LDL conjugates have been coupled to other targeting moieties such as folate (Zheng, *et al.* 2005; Song, *et al.*, 2007). These targeting agents have been reconstituted into a LDL core. Transmission electron microscopy has confirmed that these conjugates retain the size and shape of native LDL and were preferentially taken up by tumor tissues (De Vries, *et al.*, 1999). Although LDL has proven to be a useful vehicle for the delivery of lipophilic drugs and diagnostic agents to tumors, its clinical application in cancer is limited to LDL receptor related diseases because many tumors do not over express LDL receptors (Dolmans, *et al.*, 2003; Zheng, *et al.*, 2005;Fodinger, *et al.*, 2000; Bailey and Gregory, 1999).

Antibodies and serum proteins. To enhance tumor selectivity. Antibodies can be used as targeting vehicles when being conjugated to PS (Mayo, *et al.*, 2003). The conjugation of a PS to an antibody retains the photosensitizing properties and the conjugates bind to targeted cells more strongly than the native PS. Bhatti etal (Bhatti, *et al.*, 2008) introduced a system in which multiple PS were covalently attached to single chain variable fragments. The resulting photoimmunoconjugates not only retained photophysical properties but also were more potent than any of the individual PS with respect to tumor cell killing capacity. Another study showed that multiply loaded bioconjugates composed of transferrin and hematoporphyrin when combined with luminol can significantly improve the specificity and efficiency of PDT for erythroleukemic cells by a factor of almost seven fold (Laptev, *et al.*, 2006). Malatesti et al (Malastesti, *et al.*, 2006) synthesized a cationic 5,15-diphenyl porphyrin-monoclonal antibody (DPP-MAb) conjugates via an isothiocyanate linkage. The resulting DPP-Mab conjugate were photodynamically inactive. Chlorin e6-monoethylenediamine monoamide has been studied by the Hasan laboratory (Soukos et al, 1998). Theses conjugates were synthesized with various linkers including dextran, poly-L-lysine to increase the photosensitizer:MAb ratio. It was shown that ratios between 24-36 impaired immunoreactivity. These compounds also showed increased tumor selectivity and phototoxicity, yet complete removal of the tumor cells were not consistently found.

Steroids and hormones. Many steroid hormones have been conjugated to various PS to increase selectivity, based on the hypothesis that the overexpressed steroid receptors that in hormone-sensitive cancer cells can serve as the targeting site. Sharman

et al. (Sharman, *et al.*, 2004) have discussed the use and efficacy of 2-methoxyestradiol, glucocorticoids, lovastatin, estrogens, androgens, progesterone, glucocorticosteroids, thyroid hormones and retinoic acid (Golab, *et al.*, 2003; Cowled, *et al.*, 1985; Biade, *et al.*, 1993; Aranda and Pascual, 2001). All of these molecules can bind with high affinity to a specifc member of the nuclear hormone receptor superfamily (Josefen and Boyle, 2008). Steroid receptors located on the nuclear membrane attracted and directed their ligands into cancerous cells where these receptors are overexpressed.

Hormone-responsive tumor cells, especially breast tumor cells that naturally overexpress estrogen receptor, can be targeted for the selective delivery of estrogen-porphyrin conjugates for targeted PDT in breast cancer. Although many steroid-photosensitizer conjugates can effectively increase the phototoxicity within targeted tumor cells, their low binding affinity to the targeted steroid receptors remains a problem (Sharman, *et al.*, 2004). High phototoxicity often associates with low selectivity, and vice versa. For example, when chlorin e6-estradiol conjugates was introduced into the estrogen receptor positive MCF-7 breast cancer cells, it proved to be highly photoactive (James, *et al.*, 1999). However, the binding affinity of this conjugate to the estrogen receptors was about 300 times less than estradiol (Swamy, *et al.*, 2002). One the other hand, steroid-PS conjugates such as tetraphenylporphyrin-C11-β-estradiol can exhibit high selectivity toward steroid receptor positive cancer cells, but is phototoxic activity was insufficient and ineffective when being test in MCF-7 breast cancer lines (Aranda and Pascual, 2001; James, *et al.*, 1999, Swamy, *et al.*, 2002). Tamoxifen (TAM), an antiestrogen, covalently linked to pyrophenophorbide (a porphyrin derivative) via a seven

carbon long tether. Results of the estrogen receptor (ER) binding assay showed that this TAM-pyropheophorbide conjugates showed specific binding affinity for ERα and displayed a strong cell killing properties in MCF-7 breast cancer cells (Fernandez, *et al.*, 2006). In another study, four conjugates of C17-α-alkylnulestradiol and chlorin e6-dimethylester were synthesized with varying tether lengths. One of the conjugates was efficiently taken up selectively by breast cancer cells and showed were phototoxic upon irradiation with red light (Azria, *et al.*, 2009; Swamy, *et al.*, 2006).

Folate. A wide variety of photosensitizer drug carriers including liposomes, LDLs, and small oligonucleotide fragments have been conjugated to folate and evaluated for the effectiveness of folate receptor (FR) targeted delivery with varying degree of success. The cell membrane FR can be used as a selective target for PS drug delivery. The FR α isoform is usually amplified in epithelial cancers, while over expression of the FR β isoform is commonly found in myeloid leukemia and activated macrophages associated with chronic inflammatory disease (Zhao and Lee, 2008). Conjugates of folic acid can be taken up by cancer cells via receptor mediated endocytosis (Reddi, 1997). These conjugates have been shown to enhance the uptake ratio and antitumor activity of the PS both *in vitro* and *in vivo*. One of the problems with most PS currently used in PDT clinical trial is their low tumor-to-normal epithelial uptake ratio. This is especially the case with m-THPC. In order to overcome this limitation, Gravier *et al.* (Gravier, *et al.*, 2008) have reported on the synthesis of an m-THPC-like photosensitizer conjugated to folic acid. Using optical fiber fluorimetry, the enhanced selective accumulation of this

conjugate was demonstrated in FR α positive KB mouse tumor cells 4 h after injection and the resulting tumor-to-normal tissue ratio was 5:1.

FR-mediated liposomal delivery has also been shown to enhance antitumour efficacy of the photosensitizer doxorubicin both *in vitro* and *in vivo* (Pan and Lee, 2004). These FR-targeted liposomes could serve as carriers directing many genes and antisense oligodeoxyribonucleotides to FR-positive tumor cells. Both solid tumors and leukemia can potentially benefit from this approach (Reddi,1997; Pan and Lee, 2004). Studies have also demonstrated the role of folic acid conjugation in rerouting the resulting conjugate bearing an LDL carrier molecule from its natural receptor to cancer cells through folate receptors (Glickson, *et al.*, 2009; Preise, *et al.*, 2009).

Vascular targeted-PDT. To induce tumor growth, tumor tissues need to develop a vascular system based on existing host blood vessels for nutrients delivery and the removal of metabolic wastes. Vascular-targeted photodynamic therapy (VTP) makes use of the intravascular excitation of PS to produce cytotoxic ROS, which are the mediators through which VTP initiates acute local inflammation inside the illuminated area accompanied by tumor cells death (Reddi, 1997). Unlike other PDT techniques, PS used in VTP are activated in the vasculature. Various mechanisms of VTP-mediated tumor eradication through immune response induction has been examined. Using the PS WST-II, Preise *et al.* (Fleshker, *et al.*, 2008) has shown that long-lasting systemic antitumor immunity was induced by VTP that activates both cellular and humoral components and that VTP can be used in conjunction with immunotherapy for the enhancement of host antitumor immunity. To increase the overall success rate of VTP, an assessment for

successful VTP of solid tumor 24 h post treatment is needed to allow for a second treatment in case of failure. For example, the treatment of carcinoma tumors in mice by VTP with the photosensitizer WST-II was used to enable fast assessment of treatment success after 24 h. The mice that signified treatment failure, featuring various levels of subsequent tumor re-growth, were treated again and the overall successful VTP rate increased to over 90% (Eggener and Coleman, 2008). Two common vascular-targeting photosensitizers being clinically used today are verteporfin and palladium bacteriopheophorbide (WST09 or Tookad) (Trachtenberg, *et al.*, 2008). It was shown that Tookad-VTP can produce large avascular regions in the irradiated prostate, resulting in a complete negative biopsy response at high light doses (Di Stasio, *et al.*, 2005).

Lectins and saccharides for PS conjugates. Lectins are cell adhesion molecules that have been known to play a role in recognizing cell surface carbohydrates of cancer cells, including liver, breast, prostate, lung, and bile duct cell types. Thus, they are popular targets for developing glycoconjugated photosensitizer drugs (Frochot, *et al.*, 2003). Cancer cells generally overexpress monosaccharide transporters at the surface of their plasmic membrane (Taquet, *et al.*, 2007). This will allow for increased PS solubility and enhanced selectivity. Mono-glucosylated porphyrins and mono-glucosylated chlorin e6 have been shown to accumulate mainly inside the endoplasmic reticulum in human colon adenocarcinoma cell line HT29. Improved cellular uptake and increased photodynamic activity in terms of singlet oxygen quantum yield and a high extinction coefficient value were also demonstrated (Zheng, *et al.*, 2001; Chen, *et al.*, 2004). In another experiment, β-galactose was conjugated to the PS, purpurinimides. This PS-

saccharide complex is recognized by galectin-l *in vitro* and exhibits an increase in photodynamic efficacy (Hamblin, *et al.*, 2000). Non-hydrolyzable saccharide-porphyrin conjugates have also been synthesized using a tetra(pentafluorophenyl)-porphyrin and a thiol sugar derivative. These saccharides-porphyrin conjugates showed a varying degree of PDT success across different types of malignant cancer cells (Sutton, *et al.*, 2002).

Targeting with peptides. Peptides are of interest for targeted PDT due to their cell penetrating properties and their affinity to specific receptors (Taquet, *et al.*, 2007). Peptide-PS generally retain the photophysical properties of the PS, yet the quantum yield of singlet oxygen is often lowered (Taquet, *et al.*, 2007). The arginine-glycine-aspartic acid (RGD) peptide motif has been shown to improve PDT targeting efficiency and reduce the side effects of accumulated photosensitizers in non-target tissue (Taquet, *et al.*, 2007). RGD conjugated to tetraphenylchlorin (TPC) was shown to be internalized 80-100 more times than TPC alone after 24 h and it was shown to bind specifically to the overly expressed avß3 integrin on the surface endothelial cells in tumor neovasculature. But the RGD-TPC had a two-fold decrease in singlet oxygen production. Cyclic RGD peptide conjugated to photosenstizer PpIX was shown to have an increase cell accumulation over PpIX, but when tested *in vivo* it accumulated in the liver and did not enhance PDT (Taquet, *et al.*, 2007). In another study, Frochot *et al.* (Zheng, *et al.*, 2001) synthesized a conjugate of porphyrin and the avß3 integrin specific peptide RGD. The higher photodynamic efficiency observed was correlated with greater cellular uptake of the conjugate. *In vitro* results have confirmed that PS with linear or cyclic RGD motifs are much more potent in targeting tumor endothelial cells due to its high affinity to avß3

integrin receptors commonly found in many types of cancer and may potentiate the effect of vascular PDT *in vivo* as well.

The RGD motif has also been employed in PDT that involves tumor targeting with adenoviral proteins because the penton base of the adenovirus type 2 capsid protein contains the RGD sequence. Allen, *et al.* (Taquet, *et al.*, 2007) has covalently coupled the PS tetrasulfonated aluminum phthalocyanine (AlPcS4) to various adenovirus capsid proteins, and the AlPcS4A protein complex has been shown to induce greater phototoxicity than the unconjugated AlPcS4A. This suggests that the high affinity RGD/receptor complex can be potentially used as another targeting vehicle to deliver photosensitizers to the appropriate tumor cells.

Peptides can also be used to target a specific subcellular compartments. Nuclear localization sequence (NLS) has been used to target the nucleus although attempts to detect the PS-NLS in the nucleus have failed (Taquet, *et al.*, 2007). A major issue with PS-peptide conjugates *in vivo* is their lack of stability in the bloodstream (Taquet, *et al.*, 2007)**.**

Nanoparticles. Two general strategies exist for using nanoparticles as a photosensitizer carrier system. The first is using biodegradable nanoparticles, made of polymers readily degraded in a biological environment, in which the photosensitizers can be released from the nanoparticle and irradiated to produce single oxygen. The secondly strategy is to use non-biodegradable nanoparticles in which the photosensitizer is not necessarily being released from the system, but the singlet oxygen could diffuse freely in and out of the nanoparticle carrier system (Spenlenhauer, *et al.*, 1989).

One of the most commonly used biodegradable nanoparticle is the aliphatic polymer poly(DL-lactic-co-glycolide) (PLGA) nanoparticle. The mechanism of which involves a size-dependent hydrolytic process. Nanoparticles of less than 300 μm in diameter undergo a homogeneous degradation while larger particles show a heterogeneous degradation *in vivo* and *in vitro* (Gomes, *et al.*, 2005). Polymeric PLGA nanoparticles have been loaded with various PS including bacteriochlorophyll-a (BChl-a) (Gomes, *et al.*, 2007; McCarthy, *et al.*, 2005), p-THPP, m-TPPPL, m-TTP (Ricci-Junior and Marchetti, 2006), zinc(ll) phthalocyanine (ZnPc) (Zeisser-Labouebe, et al, 2006), hypericin (Hy) (Kopelman, *et al.*, 2005). The delivery process has been shown taking place in two steps: (1) adhesion of the particles to the cell surface followed by (2) the release of the PS, which caused detectable photodamage of the targeted cellular surface after laser irradiation (Bechet, *et al.*, 2008). PLGA nanoparticles loaded with p-THPP achieved vascular targeted PDT, they are limited in their loading capacity (Taquet, *et al.*, 2007). In addition, these nanoparticles lose their PS content in aqueous solution at a steady rate (Taquet, *et al.*, 2007).

Many non-degradable nanoparticles have also been synthesized, although their application in targeted PDT is still limited. The ability of non-biodegradable nanoparticles to serve as multifunctional platforms proved to be quite effective in the diagnostic and treatment of cancer. For example, in a brain cancer study (Sutton, *et al.*, 2002), a non-degradable polyacrylamide nanoparticle platform containing Photofrin® with a PEG surface coating, and the cellular targeting agent (the integrin-targeting RGD peptide) was synthesized. This multifunctional nano-platform was capable of diagnosing

brain cancer due to the presence of an associated magnetic resonance imaging (MRI) contrast enhancer. In *in vivo* experiments, the MRI contrast agent could be used to monitor changes in tumor diffusion, tumor growth and tumor load (Ahmad and Mukhtar, 2000). Treatment with this PS-nanoparticle system was followed by irradiation of the PS and tumor necrosis (Sutton, *et al.*, 2002; Ahmad and Mukhtar, 2000). Most non-degradable nanoparticles are silica-based or metallic-based. One advantage of metallic-based nanoparticles, in contrast to their silica-based counterparts, is that they can be confined to an extremely small particle size of only a few nanometers while their large surface area can facilitate a large number of photosensitizer molecules, which resulted in an increased singlet oxygen diffusion (Doughtery, *et al.*, 1998).

Folate Directed, Protein Based Targeted PDT

Our laboratory aims to develop a third generation PDT agent that will provide increased selectivity for tumor cells, and a greater concentration of PS at the site of action, using a L.E.D. light source. We will generate folate directed PDT agents that will target the FR on cancerous cells. Many cancers overexpress the FR, therefore attaching folate to a PS should enhance selectivity, and delivered into the cell via receptor mediated endocytosis.

In addition to poor specificity, the light needed to activate many PDT agents can only penetrate tissues between 0.5-3 cm. This drastically limits the types, size, and location of cancers that can be treated. Utilizing a PS that has absorbances in the optimum therapeutic window, 600-800 nm, with high extinction coefficients, will allow for deeper tissue penetration of light and enough energy to produce singlet oxygen. Our

PS of choice is Chlorin e6 (Ce6), a relatively inexpensive commercially available dye. Ce6 will lead to significant cellular death due to its absorption maxima at 660nm and corresponding high extinction coefficient of 59,000 $M^{-1}cm^{-1}$ at that wavelength. This will allow for deeper penetration into cells and higher generation of singlet oxygen.

We will use bovine serum albumin (BSA) as our carrier. Folate and Ce6 will be covalently bound to BSA through amidation reaction. The incorporation of BSA will increase solubility and reduce hydrophobicity.

CHAPTER TWO

PURPOSE OF RESEARCH

The main objective of this research is to develop a folate-directed, protein-based photodynamic therapy agent to treat cancerous tumors and to show their effectiveness in cell culture and *in vivo*. We aimed to develop novel photodynamic therapy (PDT) agents that specifically target cancerous cells. PDT utilizes oxidative damage to kill these cells. Light excites a photosensitizer, which then reacts with oxygen to form a highly reactive oxygen species, singlet oxygen. This singlet oxygen reacts with cellular macromolecules to cause lethal damage (Vrouenraets, *et al.*, 2003). We hypothesize that folate (FA) conjugation to a photosensitizer will increase the agent's specificity. Folate receptors are overly expressed in epithelial, ovarian, cervical, breast, lung, kidney, colorectal, and brain tumors (Zwicke 2012; Parker 2005) Therefore, FA-PDT has double selectivity due to the combination of folate-targeting plus limited-area light exposure. The folate containing conjugate can be taken up by the cell into the cytoplasm via receptor mediated endocytosis.

In addition to poor tissue specificity of many PDT agents, the light needed for excitation can only penetrate tissues between 0.5-3cm (Vrouenraets, *et al.*, 2003). This drastically limits the types, size, and location of cancers that can be treated. Utilizing a photosensitizer that have absorbances at longer wavelengths in the optimum therapeutic window, 600-850 nm, with high extinction coefficients, will allow for deeper tissue

penetration of light and enough energy to produce singlet oxygen (Vrouenraets, *et al.*, 2003). We hypothesized that using chlorin e6 (Ce6), a relatively inexpensive commercially available dye, as a photosensitizer will lead to significant cellular death. Ce6 has an absorption maximum at 660 nm and corresponding high extinction coefficient of 59,000 $M^{-1}cm^{-1}$ at that wavelength (Dolmans, *et al.*, 2003). This will allow for deeper penetration into cells and higher generation of singlet oxygen.

Both FA and Ce6 are hydrophobic therefore, we hypothesize by covalently attaching FA and Ce6 to bovine serum albumin (BSA), hydrophilicity will increase making conjugation chemistry more efficient and delivery to cancerous tumors easier. We choose BSA due to its relative stability, low cost, ease of purification, and its high number of lysine residues. BSA has between 30-35 free lysines, whose primary amine residues can react with the carboxyl groups, 2 and 3, respectively on FA and Ce6 to form a stable amide bond. The large number of sites of conjugation provides a platform to deliver a greater of number of Ce6 to the cancerous tumor.

HeLa cells are an immortal cell line that was derived from cervical cancer cells. This cell line is commonly used in cancer research along with a host of other scientific quests. Low and Leamon proved in 1991 that the folate receptor on HeLa cells can be exploited to deliver folate conjugated macromolecules into the cytoplasm via receptor mediated endocytosis. They also proved that macromolecules in the range of 13.7 kDa (RNase) to 443 kDa (ferritin) can be internalized into HeLa cells via the folate receptor. Therefore, we hypothesize that our folate targeted compound, FA-BSA-Ce6, which is well within the size range they explored, should be able to be internalized into HeLa

cells, thus making HeLa cells a viable option for cell culture studies. We will explore both concentration and light energy, to determine optimal experimental conditions.

In addition to cell culture, this dissertation will also discuss the use of zebrafish for targeted PDT. During embryogenesis zebrafish undergo rapid cell division, which can be used as a model for cancer. Zebrafish provides a high throughput organism for in vivo studies, as well as their transparent nature allows for insight that cannot be achieved with cell culture alone. This use may lead to a new tool for studying zebrafish development.

This body of work details the synthesis and characterization of folate targeted, protein based conjugates, their efficacy in HeLa cell culture, the elucidation of the gene expression pattern and confirmation of the folate receptor in zebrafish, and the selective targeting of cells during the first 5 days post fertilization of zebrafish embryos.

CHAPTER THREE

BSA BASED, FOLATE DIRECTED PHOTODYNAMIC THERAPY AGENT'S EFFECTIVENESS IN HELA CELLS

Introduction

Chemotherapy is one of the most popular course of treatment for cancer. It is often coupled with radiation and/or surgery as a two pronged approach to eradicating the cancer. There are over 100 chemotherapy drugs available and most work by stopping or slowing the growth of rapidly dividing cells throughout the body. This robustness makes chemotherapy very effective against cancerous cells yet it also provides an avenue for healthy cells to be negatively affected. This leads to numerous unwanted side effects. As an alternative to chemotherapy or a method to use less chemo drugs, photodynamic therapy (PDT) has become an attractive option. PDT utilizes oxidative damage to kill cells. Light excites a photosensitizer (PS), which activates oxygen to form highly reactive oxygen species (ROS), including singlet oxygen, $^1O_2$. ROS then reacts with cellular macromolecules to cause lethal damage (Ahmad and Mukhtar, 2000). In the ground state PS have two paired, opposite spin electrons. Upon light activation, one electron is promoted to a higher energy orbital, and the PS becomes excited (Robertson, 2009). The PS can return to a relaxed state by emitting energy as fluorescence. Another option is for the PS to undergo intersystem crossing. Intersystem crossing takes the PS to

an excited triplet state and from there the PS can participate in two types of reactions Type I and Type II (Robertson, 2009). Type I reaction involves the excited PS interactingdirectly with a substrate, such as the cell membrane. In this case a hydrogen atom is transferred and radicals are formed. These radicals interact with molecular oxygen to form reactive oxygen species (Robertson, 2009). In Type II reactions the excited PS transfers its energy directly to oxygen to form singlet oxygen, $^1O_2$ (Robertson, 2009). This $^1O_2$ is toxic to cells and leads to cellular death. Type II reactions are the most beneficial to combat cancerous cells because the oxygenated products that are produced are more predictable and leads to direct death of the intended cell (Robertson, 2009).

Currently Photofrin® (Porfimer sodium) is the most widely used, FDA-approved PDT drug for cancer. Photofrin® is a second generation PS that is comprised of a mixture of hematoporphryin derivatives. Photofrin® is used to treat esophageal and endobronchial cancer. It absorbs light at 635 nm and it is not very selective for cancerous cells. This is the case for most of the approved PDT drugs. Many of them have significant limitations, primarily low specificity, which causes harm to bystander cells (Dougherty, *et al.*., 1998). They rely on differences in physical properties, such as cellular pH, to discriminate between healthy and cancerous cells which leads to poor targeting of tumor. In addition, as is the case with Photofrin®, the light needed to excite many PDT agents only penetrates tissues to a depth between 0.5-3cm beneath the skin (Fuchs and Thiele, 1998). This limitation leads to significant limitation of the types, size, and location of cancers that can be treated.

Utilizing a photosensitizer that has absorption at longer wavelengths in the optimum therapeutic window, 600-850 nm, with high extinction coefficients, will allow for deeper tissue penetration of light and enough energy to produce singlet oxygen (Fuchs and Thiele, 1998). Chlorin e6 (Ce6), a relatively inexpensive commercially available dye, as a photosensitizer will lead to significant cellular death. Ce6 has an absorption maximum at 660 nm and corresponding high extinction coefficient of 59,000 $M^{-1}cm^{-1}$ at that wavelength (Oseroff, *et al.*., 1986). This will allow for deeper penetration into cells and higher generation of singlet oxygen.

To increase selectivity and effective we propose using folate (FA) as a targeting agents for the PS, Ce6. Many malignant cells overexpress folate receptors in order to support its rapid cell division and growth (Bisland, *et al.*., 1999). FA conjugation to a PS will increase the agent's specificity. Therefore, FA-PDT has double selectivity due to the combination of folate-targeting plus limited-area light exposure. The folate containing conjugate can be taken up by the cell into the cytoplasm via receptor mediated endocytosis.

Both FA and Ce6 are hydrophobic. Therefore, in order to increase solubility and reduce hydrophobicity as well as provide a scaffold for multiple molecules of Ce6 to be delivered to the cancerous cells, we covalently linked FA and Ce6 to bovine serum albumin (BSA).

Materials and Methods

Reagents.1-ethyl-3-(3dimethylaminopropyl)carbodimide (EDC), bovine serum albumin (BSA), anhydrous dimethyl sulfoxide (DMSO), ethanolamine, fetal bovine

serum, folate (FA), Hepes buffered saline (HBS), N-hydroxysuccinimide (NHS), Roswell Park Memorial Institute (RPMI), and trypsin/EDTA were purchased from Sigma Chemical Company (St. Louis, MO). Chlorin e6 (Ce6) was purchased from Frontier Scientific (Logan, UT). Cell Titer Blue Assay was purchased from Invitrogen (Grand Island, NY). HeLa cells were obtained from Dr. Stefan Kanzok's laboratory at Loyola University Chicago. All other chemicals used were analytical grade and used without further purification, unless otherwise specified.

Synthesis of BSA-Ce6, BSA-FA, & FA-BSA-Ce6. Ce6 and FA both contain multiple carboxyl groups (three and two respectively). BSA is a 67 kDa single polypeptide that has 60 lysine residues. Of the 60 lysine residues, 30-35 are available to react (Huang and Kim, 2004). Carbodiimides are commonly used to activate carboxyl groups for conjugation to primary amines. EDC is a water soluble carbodiimide that creates a zero length linker between carboxyl and amine groups. EDC coupled with NHS reacts with the carboxyl groups on Ce6 and FA to form a semi-stable NHS- ester intermediate (Han and Kim, 2004). The lysine residues (primary amine) on BSA reacts with the ester intermediate to form an amide bond (Montalbetti and Falque, 2005).

Ce6 was placed inside of a 1.5 mL microcentrifuge tube that was covered with foil. The dye was dissolved in 200-300 µl of dry DMSO. Next, it was incubated with a 10-fold molar excess of EDC and a 20-fold molar excess NHS at room temperature for 30 min. A 20-fold molar excess of the esterified Ce6 was added dropwise to BSA (10mg/ml) that was previously dialyzed in bicarbonate buffer at pH 8.0 The mixture was incubated for 24 h at room temperature and quenched with ethanolamine. FA-BSA was

prepared in the same manner as BSA-Ce6 with the only exception being that a 10-fold molar excess of FA was added to BSA. The excess Ce6, FA, NHS and ethanolamine was removed by dialyzing overnight in phosphate buffered saline (PBS) at pH 7.4.

The synthesis of FA-BSA-Ce6 (Figure 8), begins with preparing BSA-FA as described above. BSA-FA was exhaustively dialyzed in bicarbonate buffer at pH 8.0. Post dialysis a 5, 10, 15, 20, or 30 fold molar excess of esterified Ce6 was added to aliquots BSA-FA to determine the optimum Ce6:BSA ratio. The mixtures were incubated for 24 h at room temperature. The excess Ce6, NHS and ethanolamine was removed by dialyzing overnight in PBS at pH 7.4.

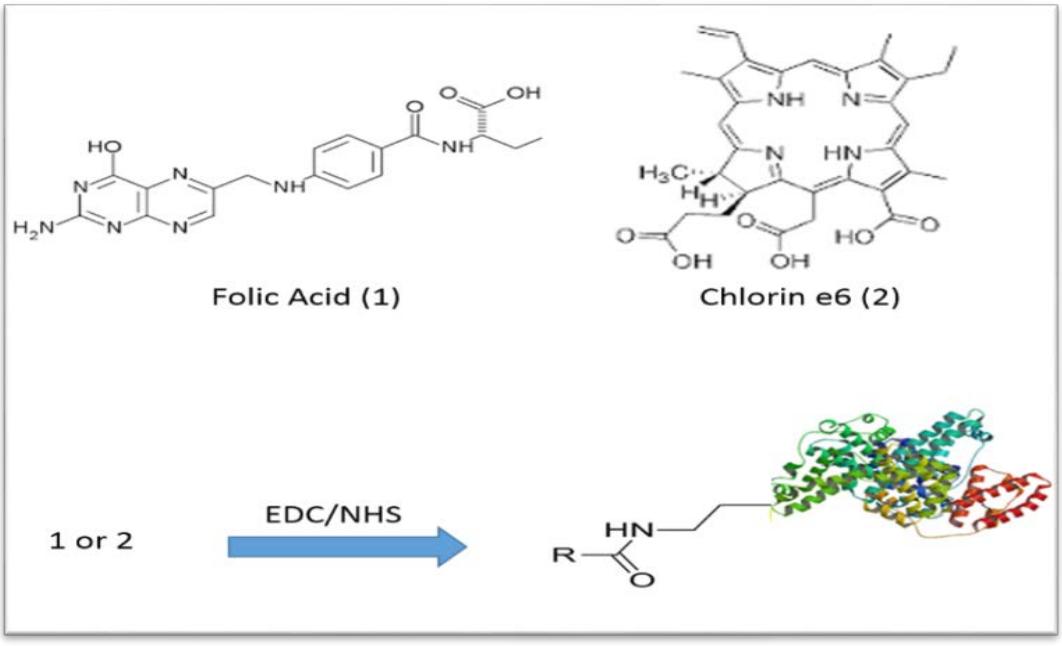

Figure 8. Conjugation Schematic. Addition of Folic Acid/Chlorin e6 to BSA. Carboxyl groups on folic acid are esterified by reacting with EDC/NHS. The newly formed ester reacts with the amine on the lysine residues of BSA to form an amide bond.

Characterization of conjugates. An acid-acetone precipitation was carried out on FA-BSA, BSA-Ce6 and FA-BSA-Ce6 to quantify the number the folates and dyes

covalently bound to the protein (Hamblin, *et al.*., 2000). Briefly, 500 µl of conjugate was added slowly while stirring to 5 mL of acidic acetone at 4°C for 4 h. The sample was centrifuged at 4000 g at 4°C for 10 min. After centrifuging the supernatant was discarded and the pellet was reconstituted in 5 mL of cold acetone, and centrifuged. The supernatant was visually inspected after each round of precipitation/centrifuging for hues of green and/or yellow. If the supernatant appeared colored, the sample was subjected to another round of precipitation. After four rounds of precipitation, an absorption spectrum was taken of the supernatant between 220 nm – 900 nm. The spectrum was analyzed for any significant peaks, paying close attention to the Ce6 maxima at 400 nm and 660 nm, and folate absorption maximum at 363 nm. This step was repeated until the spectra showed no significant peaks above baseline. The remaining pellet was reconstituted in 1.5 mL of PBS at pH 7.4 and dialyzed against PBS at pH 7.4 for 18h to remove any remaining acetone. An absorption spectra was taken of the dialyzed pellet, which contains the conjugate, and after correcting for BSA's slight contribution to the folate peak at 363 nm the number of FA and Ce6 molecules covalently attached to the protein was determined using folate and Ce6 maxim um absorptions, 363nm and 660nm respectively, and corresponding extinction coefficients of 6,197 $mM^{-1}cm^{-1}$ for folate (Kranz, *et al.*., 1995) and 59,000 $mM^{-1}cm^{-1}$ for Ce6 (Oseroff, *et al.*, 1986) .

Determination of ROS production. Photoactivation of Ce6 leads to the production of singlet oxygen ($^1O_2$) which is a reactive oxygen species (ROS) (Wawrzynska, *et al.*., 2010). ROS is considered to be integral in apoptotic and necroctic pathways. Ce6 has been studied for many years and is purported to have a high quantum

yield of $^1O_2$ (Douillard, *et al..*, 2009; Nelson, *et al..*, 1987, Qian, *et al..*, 1987; Mojzisova, *et al..*, 2007).To determine if FA-BSA-Ce6 maintains $^1O_2$ production, ρ-nitroso-N, N′-dimethylaniline (RNO) was used as a singlet oxygen sensor. The production of singlet oxygen was monitored by bleaching RNO at 440nm. A 250 μM RNO and 0.03M histidine solution was made in D_2O. D_2O was included to assist in extending the lifetime of $^1O_2$ (Klotz, *et al..*, 1997). 6 μM of unconjugated Ce6 or FA-BSA-Ce6 were dissolved in separate vials of 700 μl of 1% DMSO in D_2O to maintain solubility of unconjugated Ce6. Each solution was added to the RNO solution and bubbled with water-saturated oxygen for 10 min. The mixture was placed in a quartz cuvette and irradiated with 44.9 J/cm^2 (8 min) with an 660 nm LED lamp. The absorption at 440 nm (λmax of RNO) was monitored every 30 s using a UV-Vis spectrophotometer (Krajlic, *et al..*, 1978; Mosinger and Zdenek, 1997; Muller-Breitkreutz *et al..*, 1995).

Dark cytotoxicity & phototoxicity. HeLa cells were maintained in Roswell Park Memorial Institute (RPMI) media (pH 7.4), supplemented with 10% fetal bovine serum (FBS), 2 mM glutamine, and 10 mM HEPES, at 37°C with 5% CO_2. Prior to treatment the medium was switched to folate deficient RPMI medium. Cells were seeded at an initial density of 10,000 cells per well in black-walled 96-well plates. Following seeding cells were exposed to the conjugates, BSA-Ce6 or FA-BSA-Ce6, at a Ce6 concentration of 1, 2, 5 and 10 μM respectively and incubated for 24 h in the dark. After incubation the folate-deficient medium was removed and after several washes the cells were placed in folate-containing-RPMI. The cells were then irradiated with a LED lamp (660 nm) for 1, 2, 4, and 6 min, respectively to deliver 5.6, 11.2, 22.5 and 33.7 J/cm^2 respectively. In

parallel, an identical control plate was kept in the dark. After incubating for 24 h cell viability was determined using Cell Titer Blue Assay Kit (Promega).

Statistical analysis. Two-tailed student's t test was used to identify significance between means. The level of significance was set to $p < 0.05$. All values stated are reported as the mean +/- standard deviation from the mean.

Results

Quantification of folates and chlorin e6 molecules bound to BSA. Slight modification of published protocols for carboxyl to amine amide bond formation (Leamon and Low, 1992), BSA-Ce6 and FA-BSA-Ce6 conjugates were synthesized via exposed lysine residues in BSA and free carboxyl groups on Ce6 and FA (Figure 8). BSA (10mg/ml) was conjugated to folic acid (FA) using a 10 molar excess of FA to protein. Based on the absorbance after dialysis at FA maximum absorption wavelength 368 nm and corresponding extinction coefficient of 7410 $mM^{-1}cm^{-1}$ (Kranz, *et al.*., 1995) the number of folates covalently bound was determined to be two. Ce6 has an absorption maximum at 660 nm and corresponding extinction coefficient of 59,000 $M^{-1}cm^{-1}$ (Oseroff, *et al.*., 1986) at that wavelength. A UV-vis spectra was taken after the final dialysis, and the number of Ce6 molecules covalently attached to FA-BSA was determined. As shown in Table 2, 5:1, 10:1, 20:1 and 30:1 ratio of Ce6 to protein produced four, six, ten, and ten molecules covalently attached respectively.

Porphryin based dyes, such as Ce6, can potentially strongly interact non-covalently with serum proteins (Mew, *et al.*., 1983). To ensure that all excess Ce6 molecules in addition to FA were removed an acetone extraction was also performed on

each of the conjugates. After conjugation, an aliquot was added dropwise to cold acetone, and the pellet was analyzed via absorption spectroscopy. The resulting number of FA and Ce6 that were determined to be covalently attached matched the results from exhaustively dialyzing the conjugates. Based on the results, acetone extraction was deemed to be unnecessary and the conjugates were dialyzed in PBS post conjugation. Based on the results, a ratio of 20:1 was used for FA-BSA-Ce6 synthesis.

Ce6:BSA	***# of Ce6***
5:1	4.2
10:1	6.3
20:1	10.4
30:1	10.3

Table 2. Number of Dye Bound. The number of Ce6 molecules was determined using varying rations of photosensitizer to protein. Ten molecules were covalently attached using 20:1 and 30:1, therefore, 20:1 was chosen.

Singlet Oxygen Production due to photoactivation. Ce6 produces a significant amount of singlet oxygen (Fernandez, *et al.*., 1997). To determine if Ce6 maintains its output of singlet oxygen once conjugated to FA-BSA, samples of FA-BSA-Ce6 and Ce6 (both samples contained the same Ce6 concentration) were mixed with RNO (a singlet oxygen quencher) and was irradiated with a L.E.D. lamp at 660 nm for 8 min. An UV-Vis spectra was taken every 30 s monitoring the absorption at 440 nm (Figure 9). As singlet oxygen is quenched by RNO, there is a reduction in the absorption at 440nm. The decrease in the peak was monitored until the absorbance was around 0.100.

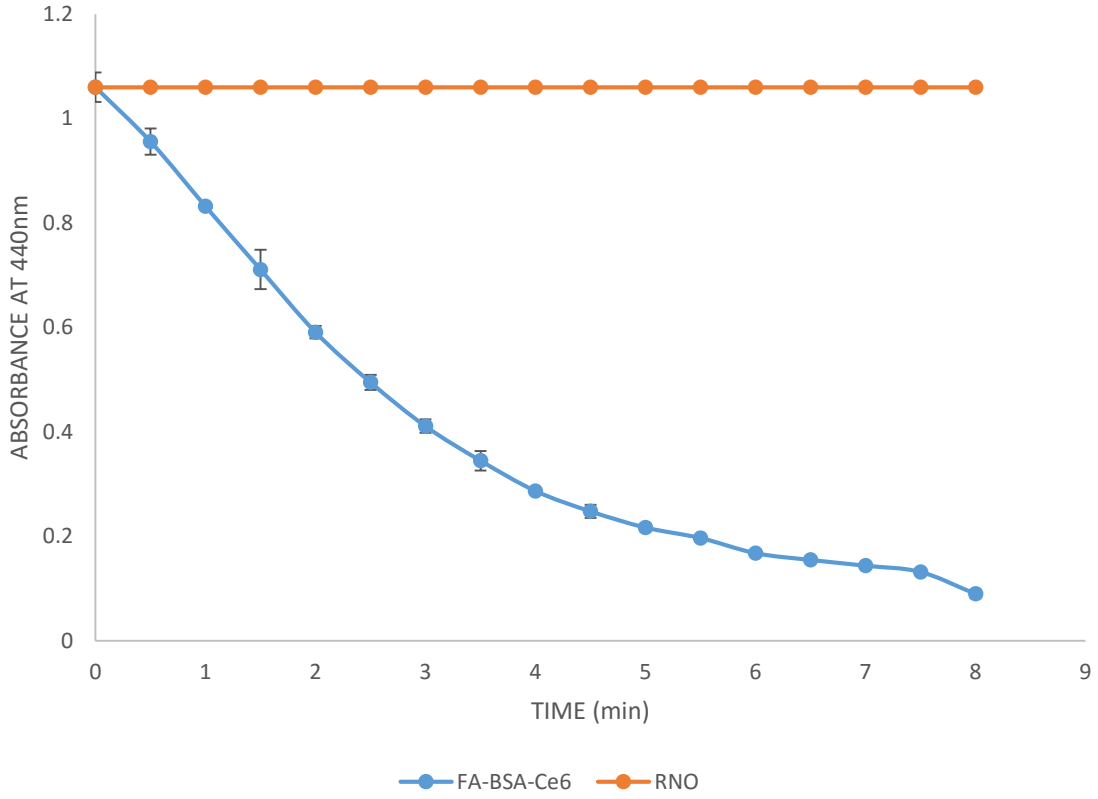

Figure 9. Singlet Oxygen Produced from FA-BSA-Ce6. Singlet oxygen quencher, RNO, was used to monitor the production of singlet oxygen of FA-BSA-Ce6 upon irradiation at 660nm between 0 min and 8 min.

FA-BSA-Ce6 dark cytotoxicity. The cells were exposed to the conjugates for 24 h, washed and then incubated for another 24 h, after which cell viability was measured using Cell Titer Blue Assay Kit (Figure 10), a fluorescence assay in which viable cells exhibit a higher fluorescence than non-viable cells. Percent survival was determined by comparison to cells exposed to media only. BSA-Ce6 at a concentration of 10 µM had a 98% (+/- 5 %) cell survival rate. FA-BSA-Ce6 at 1µM, 2 µM, 5 µM, and 10 µM concentrations were also assayed for dark cytotoxicity. The respective survival rates were as follows: 100 % (+/- 2 %), 93 % (+/- 1.5 %), 98 % (+/- 3 %), 98 % (+/- 2 %) (Figure

10). There was no statistical difference between media only cells (control) versus any of the test wells. All of the conjugates cell survival rates were above 93% when compared to control.

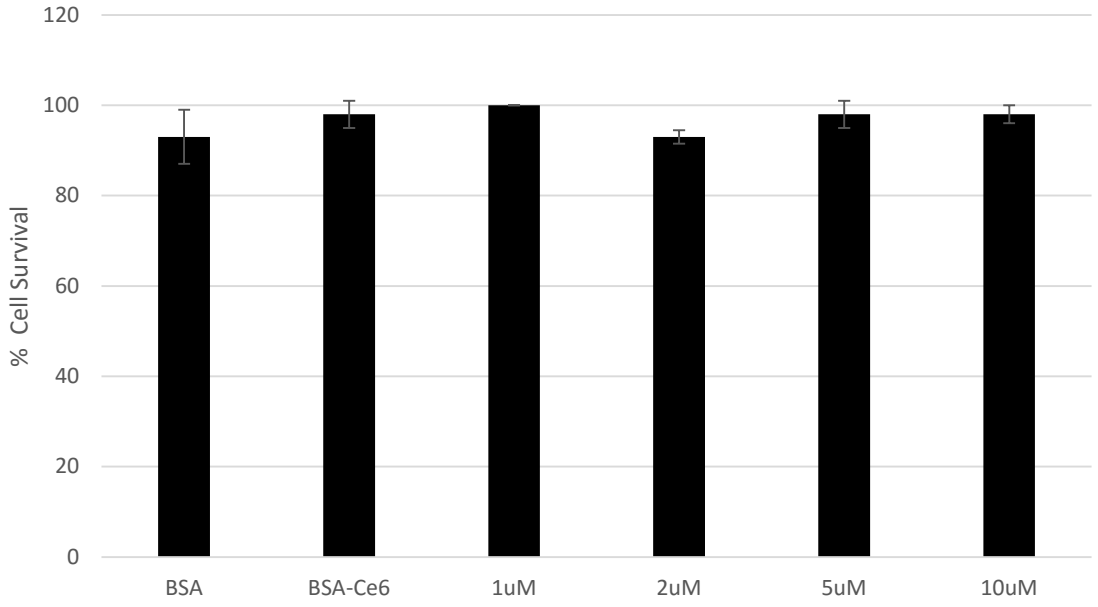

Figure 10. Dark Cytotoxicity Results of Conjugates and Controls. Based on control cells all conjugates are not significantly different.

Cell death via photoactivation of FA-BSA-Ce6. The viability of media only cells was set at 100%, and all conjugates are reported in comparison to those cells. Cell viability for 1µM, 2 µM, 5 µM, and 10 µM FA-BSA-Ce6 was assayed at 5.6, 11.2, 22.4, and 33.7 J/cm2 of light, in addition to 10 µM BSA-Ce6. Across all times of light irradiation BSA-Ce6 maintained above 92% cell survival (Figure 11).

No significant cell death resulted for 1µM of FA-BSA-Ce6 at any of the irradiation energies. The lowest viability for FA-BSA-Ce6 at 2 µM was 74% with 2 minutes of light irradiation. This was the lowest viability for that concentration, which

was significantly different than at 1 minute, but not significantly different from 4 minutes of light (based on standard deviations).

While the lowest viability for FA-BSA-Ce6 at 2 µM was 74% with 2 min of light, the highest viability for both 5 µM and 10 µM FA-BSA-Ce6 was 76% with 1 min of light. 5 µM and 10 µM samples show significant difference from the controls starting at 2 minutes of light, yet they do not show any statistical difference from one another for the other light energies (Figure 12). 5 µM FA-BSA-Ce6 caused the most cell death with 4 min of light which resulted in 5.3% cell survival. 10 µM FA-BSA-Ce6 caused the most cell death at 4 min light as well, which resulted in 3.9% cell survival.

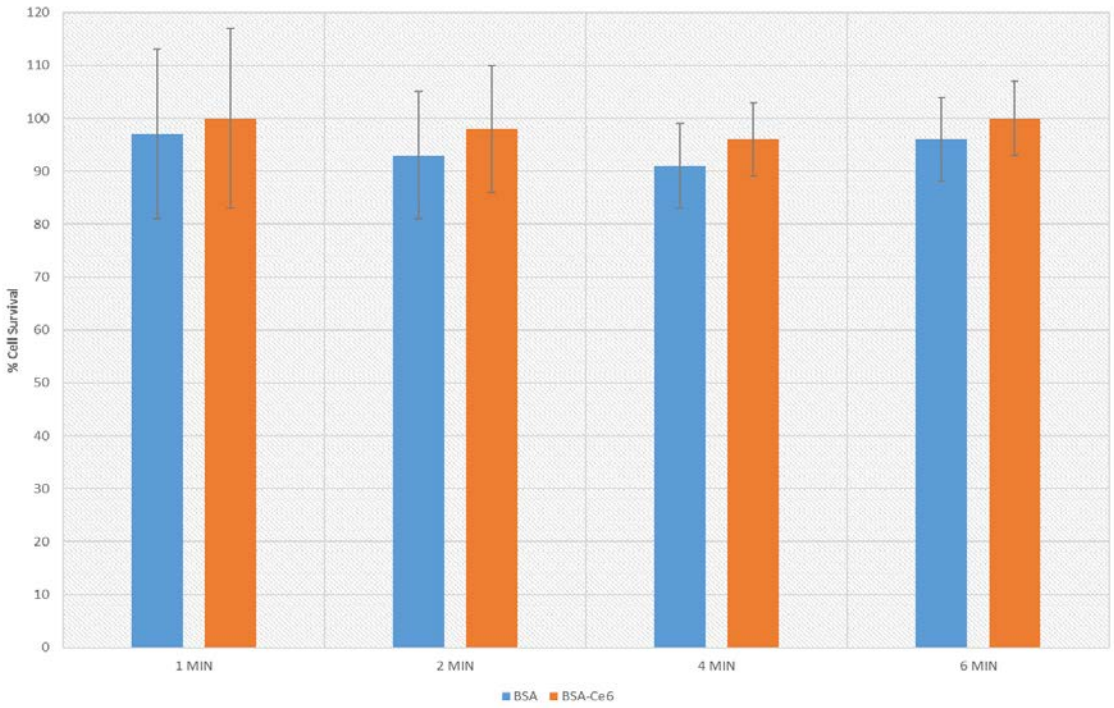

Figure 11. Phototoxicity of Controls: BSA or BSA-Ce6 showed significant cell death in comparison to cells exposed to media only.

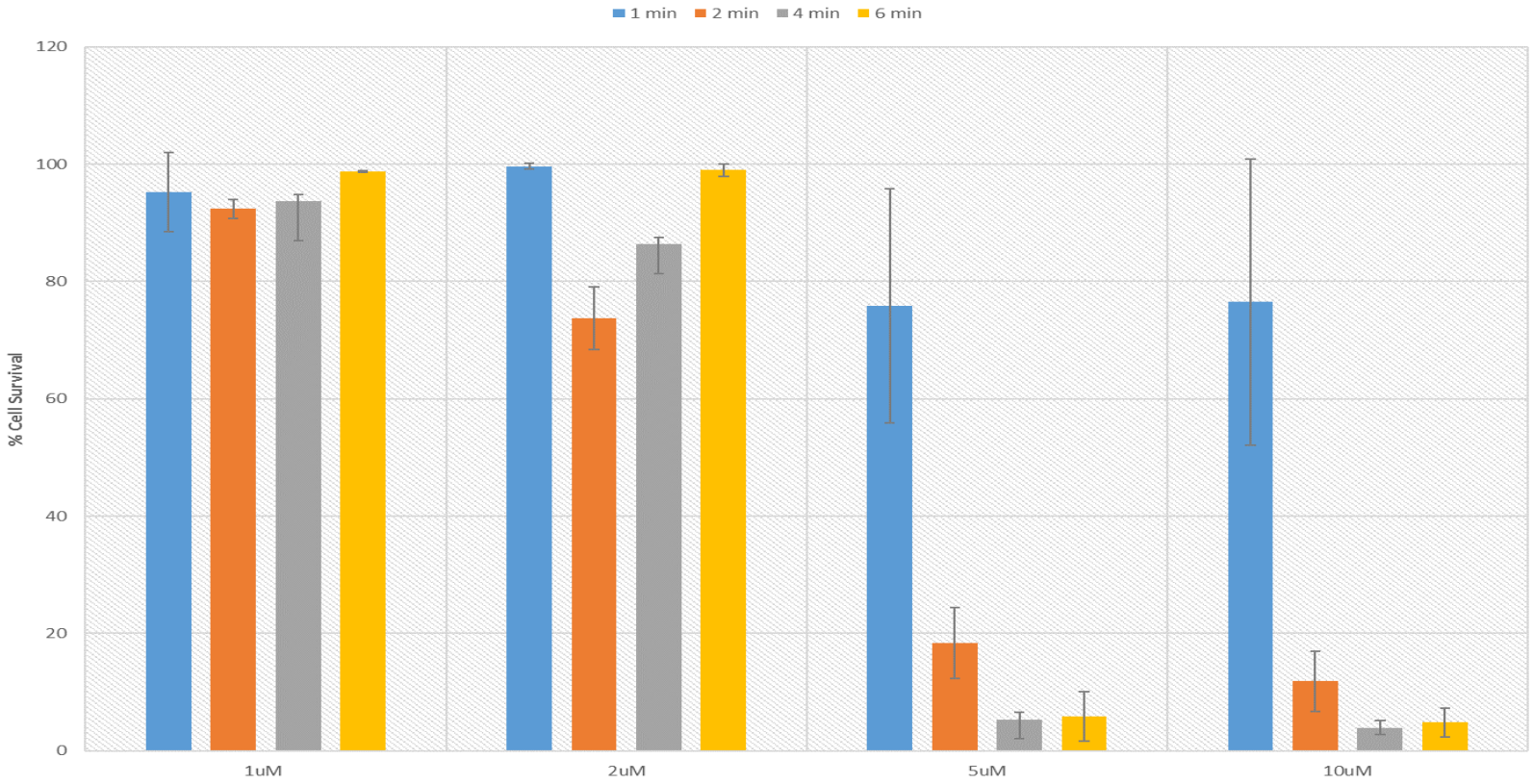

Figure 12. Phototoxicity of FA-BSACe6: Results of FA-BSA-Ce6 at varying concentrations and light irradiation times.

Discussion

An effective photodynamic therapy agent will be phototoxic but not cytotoxic in the dark. In an attempt to maximize the efficiency of Ce6 conjugation to BSA we varied the ratio of Ce6:BSA. There was a lack of increase in Ce6 conjugation with 30:1 ratio in comparison to 20:1. In 2004 Huang and Kim reported on the use mass spectrometry coupled with lysine specific cross-linkers to analyze the tertiary structure of BSA. In their study the were only able to crosslink 34 of the 60 lysines that are present in BSA (Huang and Kim, 2004). The lack of increase in Ce6 conjugation with 30:1 vs 20:1 ratio could be due to steric hindrance of the available lysines. Thus, a 20:1 ratio of Ce6 to protein was chosen, and based on UV-Vis spectra conjugation of both folate and Ce6 was successful.

To ensure that Ce6 maintained its ability to produce singlet oxygen, its production of singlet oxygen was monitored via a singlet oxygen quencher. The results from this experiment confirmed that upon conjugation to FA-BSA, Ce6 produces singlet oxygen.

The effectiveness of FA-BSA-Ce6 as a photodynamic therapy agent was examined in comparison to media-only cells and BSA-Ce6 (Figure 11). BSA-Ce6 was shown to not be phototoxic or cytotoxic at 10 μM concentration and at all light intensities assayed. This is a significant finding because free Ce6 at significantly lower concentrations have been proven to be cytotoxic and we report 98% cell survival rate of BSA-Ce6. Conjugating Ce6 to BSA increases its solubility and decreases it hydrophobicity. This is the most apparent reason why BSA-Ce6 did not show any significant cell death, while in the literature Ce6 demonstrates cytotoxicity.

As shown in Figure 12 cell survival is both concentration and light dose dependent. As the concentration of FA-BSA-Ce6 increase and as light exposure time increases, cell survival decreases. Interestingly, the same effects are not seen with BSA-Ce6 (Figure 11). Light irradiation time does not affect percent survival. The only difference between the two conjugates is the targeting moiety, folate. This data combined with the ROS production data, it can be concluded that the conjugate is being taken up via receptor mediated endocytosis.

We have demonstrated that conjugation of FA and Ce6 to BSA provides an effective PDT agent that is specifically taken up into the cells via receptor mediated endocytosis. The conjugate is both dose time and concentration dependent. Thus the higher the concentration and the longer light irradiation, the less cell survival. Concentrations less than or equal to 2 μM are not effective at killing cells in culture. In contrast there is no benefit in using 10 μM FA-BSA-Ce6 due to 5 μM FA-BSA-Ce6 providing essentially the same magnitude of cell death. FA-BSA-Ce6 offers potential benefits not seen with approved PDT agents. The main difference presented is the ability to target cells that upregulate the folate receptor. Thus combining limited light area exposure and the targeted conjugated, FA-BSA-Ce6 offers double selectivity.

In 2015 Donghong Li *et al.* synthesized a new a *m*-tetra(Hydroxyphenyl)chlorin (*m*-THPC) derivative based PS called, PS1, and covalently attached folate to PS1 via PEG. *m*-THPC is approved for use in Europe, Norway, and Iceland as PDT agent under the name Foscan (5). *m*-THPC has a maximum absorption at 650 nm and without a targeting moiety such as folate, it demonstrates poor selectively. Li reported on improved

tumor selectively over *m*-THPC without folate. HeLa cell culture experiments with 15.2 µM PS1 and light dosages up to 36 J/cm^2 resulted in cell viability for all light dosages above 10%. When the concentration was varied up to 147 µM and the light was constant at 18 J/ cm^2, cell viability was above 20% for all concentration tested. Using almost three times less of PS, and three times less light, our 5 µM FA-BSA-Ce6 with 11.2 J/cm^2 of light, produced similar results.

In another study folate-targeted PEGylated liposomes with *m*-THPC were synthesized and tested for its effectives as a PDT agent (Moret, et al., 2013). In this study the results for phototoxicity in KB cells were significantly better than *m*-THPC alone and the work PS1. Liposomes have previously been shown to be a good encapsulator and carrier of *m*-THPC (Moret *et al.*, 2013). Moret and colleagues synthesized two *m*-THPC liposome conjugates with two different PEG lengths. While no increase of uptake of was seen with the smaller 2000 kDA PEG over a zero length linker, uptake was increased with the larger 5000 kDa PEG. Their folate targeted conjugate produced less than 10% cell survival with only 2.4 µM of conjugate and .8 J/cm^2 of light. This is a significant improvement in comparison to our conjugates and PS1. But, they also discovered that the untargeted and targeted conjugates produced similar phototoxicity. Un-targeted, BSA-Ce6 was not phototoxic to cells.

Lee and Low showed that PEG lengths can affect the photo-killing capacity and uptake of PDT agents. PS1 was synthesized with a 75 kDa PEG and produced little cell death in comparison to Moret and colleagues conjugate. Laura Donahue and colleagues (unpublished) has synthesized a 2000 kDa FA-PEG-Ce6 PS that shows promise as a good

PDT agent at lower concentration than FA-BSA-Ce6, yet FA-PEG-Ce6 showed some cytotoxicity in the dark. Based on these findings with PEG linkers, it may be beneficial to link folate to BSA using a 2000-5000 kDa PEG to increase phototoxic at lower concentrations while maintaining minimal dark cytotoxicity.

CHAPTER FOUR

EXPRESSION AND FUNCTIONAL CHARACTERIZATION OF THE FOLATE RECEPTOR DURING ZEBRAFISH EMBRYOGENESIS

Introduction

Folate is a well-studied B vitamin commonly referred to as Vitamin B9. This vitamin is necessary for cell maintenance and division due to its nature as a methyl donor required for the synthesis and modification of DNA, RNA, and the amino acids serine and methionine (Choi and Mason, 2000; Keleman, 2006). Folate deficiency during human fetal development can lead to neural tube defects (Botez and Reynolds, 1979; Clarke, *et al.*., 1998; Reynolds, 2002; Seshadri, 2001). The British Medical Research Council sponsored research that showed that women who had prior neural tube defect affected pregnancy reduced the risk of having a subsequent neural tube defect affected pregnancy by 70% when they supplemented their diets with 4.0 mg per day of folic acid (Wala and Sheldon, 1991).

Interestingly, folate can be both a cancer protectant and a pro-tumor agent (Meenan, *et al.*., 1997; Willet, 1994; Giovannucci, *et al.*, 1993; Farias, *et al.*., 2015; Zwicke, *et al.*., 2012). This discrepancy seems to lie in the balance of the amount of folate in the system and its bioavailability to cells. During normal cell differentiation in humans, the ability of each cell to import folate is controlled by the protein Folate

Receptor 1 (FOLR1). In many tumor cells, the FOLR1 protein is overexpressed, suggesting a possible target for anti-cancer therapies (Yoo and Park, 2004; Briggs, 2002

The teleost *Danio rerio* (also known as the common zebrafish) has become a popular model organism for studying vertebrate development and disease due to its functionality and the relative ease with which it is possible to subject them to standard molecular, genetic, and embryological manipulation (Kao, *et al.*., 2014). As an example, many of the neural tube defects due to folate deficiency in humans have also been documented in zebrafish (Blair, *et al.*., 2005). Approximately 71% of human genes have at least one zebrafish orthologue, and 47% of these have a direct, one-to-one relationship with their zebrafish counterpart (Kao, *et al.*., 2014).

We have defined the expression pattern of zgc:165502, the zebrafish orthologue of the human FOLR1 gene, during embryogenesis using reverse transcription polymerase chain reaction (RT-PCR), and whole mount *in situ* hybridization (WISH). This expression pattern will allow researchers in multiple fields the ability to study the endogenous zgc:165502 gene as expressed during embryogenesis.

Methods

Zebrafish care and husbandry. Zebrafish were maintained at Loyola University Chicago. All studies were performed with the approval of the Institutional Animal Care and Use Committee (IACUC). Wild-type embryos were raised and staged as described in Kimmel *et al.*, 1995. Post-gastrulation stages were treated with 0.005% 1-phenyl-2-thiourea (PTU) solution to prevent melanin pigment from developing. Embryos older than 24 h post fertilization (hpf) were treated with fresh PTU solution once a day. Once

the embryos reached the desired stage, they were dechorionated manually if necessary, anesthetized with 0.2% Tricaine pH 7.0, then fixed in 4% paraformaldehyde (PFA) in PBS pH 7.0 at 4°C. After fixing, the embryos were washed four times with phosphate buffered saline with 0.1% Tween-20 (PBST). After washing, the embryos were placed in 100% methanol (MeOH) and stored at −20 °C.

Reverse-transcription polymerase chain reaction (RT-PCR). RT-PCR was performed to confirm the presence of the mRNA for the folate receptor at various stages of early embryo development: 1- to 2-cell, 256-cell, sphere, germ, shield, 1 days post fertilization (dpf), 2 dpf, 3 dpf, and 4 dpf. The primers were designed to anneal to sequences in exons on both sides of an intron. Designing the primers in this way allowed for differentiation between the PCR products that were amplified by any possible genomic DNA contamination, and those amplified by the cDNA created from the RNA template. Total RNA was isolated from 50 staged embryos using a TRIzol reagent (Life Tech) and purified using a Direct-zol kit and its corresponding protocol (Zymo Research). Of the resulting total RNA, 1.5 µg from each embryo stage was reverse transcribed using oligo-dT primers (Integrated DNA Technologies) and a SuperScript III Reverse Transcriptase kit (Life Tech) to generate first-strand cDNA. One microliter of cDNA from each stage was used as a template for the primers 5’-ATT CCT CAC CTG AGC AGA ACA TGG-3’ (forward) and 5’-TGA GGT GAG CAC TCA TAG AAG C-3’ (reverse) to amplify a 300 bp fragment of the folate receptor cDNA. The PCR was run with 35 cycles of 45 s at 95 ˚C, 1 min at the annealing temperature 62 ˚C, and 1 min at 72

˚C. Ten microliters of the PCR product was analyzed with a molecular weight marker (Hi Lo ladder, New England BioLabs) on a 1% Tris-acetate-EDTA agarose gel.

***In situ* hybridization.** The complete cDNA sequence of human gene FOLR1 was used as a query in a BLAST search of the zebrafish reference genome (Zv10). This yielded a single cDNA clone (7433953) which was obtained as a plasmid clone from Open Biosystems. The fragment was inserted into pCSdest plasmid 22423 (Addgene) and linearized using the restriction endonuclease AscI. A digoxigenin-labeled anti-sense probe was synthesized using a RNA labeling kit with SP6 RNA polymerase (Roche). The folate receptor sense RNA probe was synthesized and used as a control.

Whole mount *in situ* hybridization was carried out as presented in Sisson and Topczewski (2009) and Thisse (2000) using low stringency conditions (50% formamide hybridization buffer with a .02% Saline-Sodium Citrate Buffer (SSC) final wash). Embryos were placed in 1.5 mL micro-centrifuge tubes, and rehydrated using serial dilutions to replace MeOH with PBST (75% MeOH:25% PBST, 50% MeOH:50% PBST, 25% MeOH:75% PBST, 100% PBST). Next, embryos staged between 1 dpf and 4 dpf were digested using a solution of 1 µL Proteinase K in 2 ml PBST. Embryos that were staged at 1 dpf were digested for 5 min and embryos staged at 2 dpf and 3 dpf were digested for 30 min. 4 dpf embryos were digested for 45 min. After digestion the embryos were placed in 4% PFA for 20 min, and then transferred into PBST. The embryos were pre-hybridized for 3 h with 500 µL hybridization buffer (Hyb+) that contained: 50 mL formamide, 25 ml 20X saline-sodium citrate buffer, 5 mg heparin, 50 mg tRNA, 100 µL 0.1% Tween-20, and 460 µL l 0.1M citric acid. During pre-

hybridization the embryos were kept at 70°C. After 3 h, the embryos were removed from the incubator, and two embryos from each stage were placed in a single micro-centrifuge tube for blocking. After this, 300 µl of Hyb+ containing 500 ng of anti-sense probe was added to each tube (except for the blocking embryos) and kept at 70°C overnight. The blocking embryos were treated the same as the other samples except they were void of probe. The following day, the Hyb+ with probe was removed, and each stage was moved into 0.02% SSC by successive washes of hybridization buffer without tRNA (Hyb-) and SSC (100% Hyb-, 75% Hyb-:25% 2X SSC, 50% Hyb-:50% 2X SSC, 25% Hyb-:75% 2X SSC, 100% 2X SSC, 100% 0.02X SSC). Following the SSC washes the embryos were moved into PBST using serial dilutions. Next all of the embryos except the blocking embryos were treated with 500 µl blocking solution (20% fetal bovine serum (Life Tech), 2% bovine serum albumin (Sigma) in PBST) for 4 h at room temperature. The blocking embryos were pre-absorbed with anti-digoxigenin antibody (anti-DIG, Roche) for 4 h. After 4 h the pre-absorbed antibody was diluted with fresh blocking solution, and used to replace the blocking solution in each tube. The tubes were placed in the dark overnight at 4 °C. The next day the embryos were washed several times with PBST and freshly made staining buffer (0.100M Tris-HCl (pH 9.5) (Sigma), 0.100M NaCl (Sigma), 0.1% Tween 20 (Sigma)). Following the washes the embryos were stained with 5-bromo-4-chloro-3'-indolyphosphate (BCIP) and nitro-blue tetrazolium (NBT) staining solution (Roche) and placed in the dark at room temperature. The embryos were monitored closely for staining and after defined stains developed, the embryos were washed multiple times with stop

solution (0.5M EDTA in PBST). The resulting embryos were imaged using a Nikon digital camera fitted to a light stereo microscope using 3.2X magnification.

Synthesis of folate-bovine serum albumin-rhodamine (FA-BSA-RH). FA-BSA-RH was synthesized as shown in Figure 13. 10 mg of folate (FA) was placed inside of a small, foil-wrapped Eppendorf tube and dissolved in 200-300 µl of anhydrous dimethylsulfoxide (DMSO). This solution was then incubated with a 10-fold molar excess of 1-ethyl-3-(3-dimehtylaminopropyl) carbodimide (EDC) and a 20-fold molar excess of N-hydroxysuccinimide (NHS) at room temperature for 30 min. The resulting esterified or "activated" FA was added to a 10-fold molar excess of bovine serum albumin (BSA) previously dialyzed in bicarbonate buffer at pH 8.0. The mixture was incubated for 24 h at room temperature and quenched with ethanolamine. The excess FA, NHS, and ethanolamine was removed by dialyzing overnight in bicarbonate buffer at pH 8.0. Rhodamine B isothiocyanante (RH) was placed inside of a small foil-wrapped Eppendorf tube dissolved in 200-300 µl of anhydrous DMSO. A 10-fold molar excess of RH was added to the FA-BSA solution that was previously dialyzed in bicarbonate buffer at pH 8. The mixture was incubated for 24 h at room temperature and quenched with ethanolamine. The excess Rhodamine B was removed by dialyzing overnight in PBS at pH 7.4 in the dark.

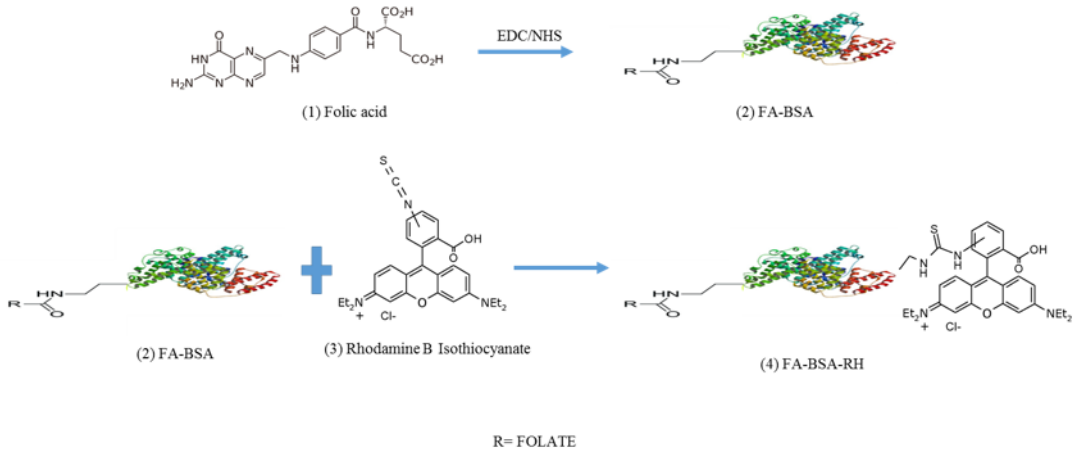

Figure 13. Synthesis Scheme of FA-BSA-RH. Folic acid (1) was reacted with EDC/NHS to yield "activated" folic acid. Activated folic acid was reacted with lysine residues on BSA to yield FA-BSA (2). (2) was reacted in buffer with RH (3) to yield the final product FA-BSA-RH (4).

Uptake of FA-BSA-RH. Wild type zebrafish embryos were collected at 3 dpf. Three embryos were placed in a single well that contained 3 ml of either embryo media, BSA in embryo media (50 µM), 50 µM BSA covalently attached to rhodamine (a red fluorescent dye) (BSA-Rh), or 50 µM BSA covalently attached to rhodamine and folate (FA-BSA-Rh). The wells were placed in a 37°C incubator overnight in the dark. After 24 h, the solutions were removed and the embryos were washed 3X with embryo media and returned to the incubator for 24 h. A total of 20 embryos were assayed with each conjugate (BSA, BSA-Rh, FA-BSA-Rh) and embryo media. Fluorescent images were taken of each embryo after washes and 24 and 48 h after exposure to the conjugates with a stereo fluorescent microscope with 3.2X magnification.

Results and Discussion

Conservation of the folate receptor between species. As we are interested in utilizing zebrafish as a model of FOLR1 protein structure and function, we first set out to

determine if the zebrafish zgc:165502 protein was similar to its orthologues. To do this, we obtained sequences for 11 identified or predicted chordate Folr1 proteins spanning from *Ciona intestinalis* to *Homo sapiens*, about 750 million years apart in evolution, to generate a phylogenic tree (Hedges, *et al.*., 2015; Shen, *et al.*., 2012). We also included the two known *human* paralogs of FOLR1, FOLR2 and FOLR3, in our comparison as an out group (Figure 14). Our tree demonstrated that the Folr1 proteins seem to follow the predicted vertebrate gnathostome phylogenetic order with higher amino acid conservation being observed within a subclass or clade of animals (see Neopterygii and Mammalia in Figure 14). Interestingly, the Folr1 amino acid identity conservation is ~50 % for animals whose last common ancestor existed about 435 million years ago (Shen, *et al.*., 2012, Antony, 1996).

The human FOLR1 protein is composed of multiple domains that have been well characterized for their biological functions (Zhao, *et al.*., 2011; Lee, *et al*., 2011). These domains include an endoplasmic reticulum (ER) signal peptide that is cleaved away after protein synthesis, a folate receptor family domain (FRF), a glycosyl-phosphatidyl-inositol (GPI) site, and a transmembrane helices domain (THD, Figure 15). We determined the percent identity and percent conservation for each of these domains between the human FOLR1 and other vertebrates, including zebrafish (Figure 15). For this comparison we used 7 species with published full-length Folr1 proteins.

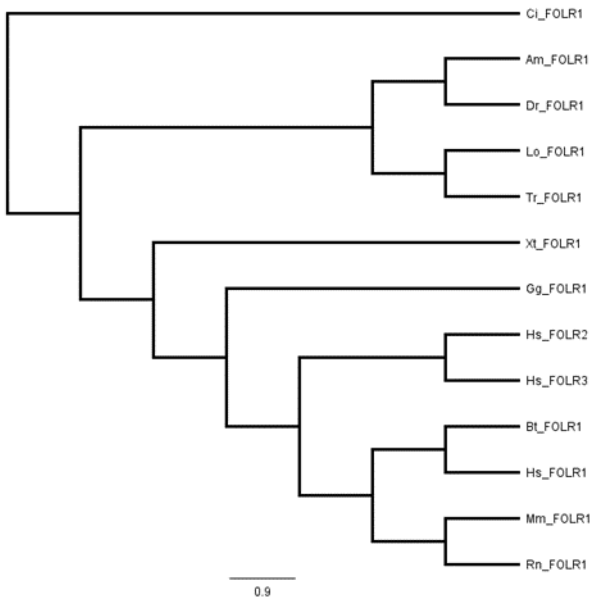

Figure 14. Phylogenetic Tree. FOLR1 proteins follows the predicted vertebrate gnathostome phylogenetic order with higher amino acid conservation being observed within a subclass or clade of animals.

Of the four domains, the FRF domain had the highest percent identity at 58%. Interestingly, many of the amino acids that were conserved between human and zebrafish were also found to be conserved in the other vertebrates looked at, suggesting the importance of these amino acids. Of particular interest, within the human FOLR1 FRF domain are two regions that interact with folate: Folate Binding Sites (FBS) 1 and 2. The human FOLR1 FBS1, amino acids 124-128, consists of WRKER. When compared to zebrafish, only one amino acid is different (K126 →R), which conserves the basic charge needed at that location. The human FBS2, at amino acids 157-162, consists of HKGWNW. Again, only one amino acid is different between human and zebrafish FOLR1 protein in this region. Asparagine 161 has been changed to aspartate acid, both of which are polar. While this change does result in a negative charge at this location it is

interesting to note that five of the nine species looked at have aspartic acid at this location while the other four have asparagine. Taken together, the high conservation of chordate Folr1 proteins and the conservation of critical functional domains between zebrafish and human FOLR1 protein, suggest that the zebrafish Folr1 receptor is a good candidate to study aspects of vertebrate Folr1 protein function.

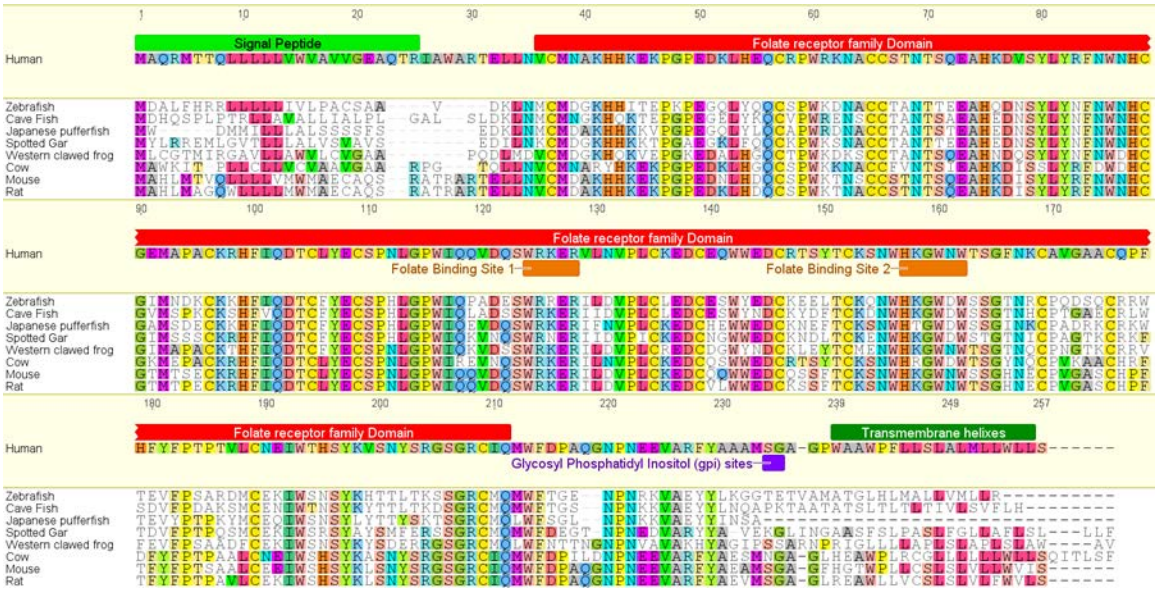

Figure 15. FOLR1 Domains. Percent identity and percent conservation for domains between the human FOLR1 and other vertebrates, including zebrafish .

Zebrafish zgc:165502 is a maternally loaded gene that is present during the first 4 days of development. To map the expression of the zebrafish folate receptor, we used reverse transcription-polymerase chain reaction (RT-PCR) on total RNA prepared from the following zebrafish stages: 1- to 2-cell, 256-cell, sphere, germ, shield, 1 dpf, 2 dpf, 3 dpf, and 4 dpf. Amplification with the designed primers yielded a single band at the predicted size of 300 bp (Figure 16) for all stages assayed.

Expression was seen before the zebrafish maternal-zygotic transition at the 512-cell stage (~2.75 h post fertilization), this suggests that zgc:165502 mRNA is maternally loaded. These findings correlate with previous research demonstrating that multiple genes in the folate metabolic pathway are also present as early as the 1- to 2-cell stage in (Lee, *et al.*., 2012).

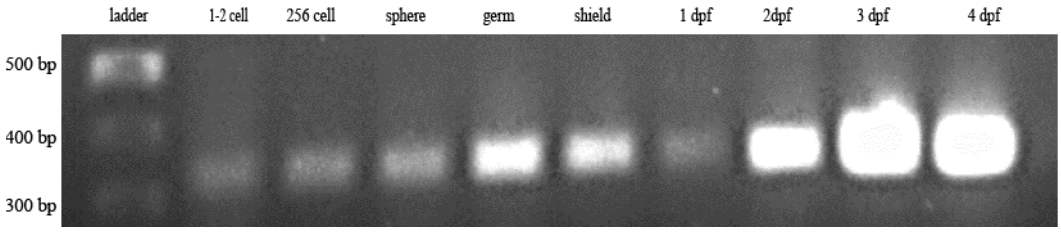

Figure 16. RT-PCR Results. zgc:165502 is detected in embryonic stages of zebrafish by RT-PCR. Each stage assayed presented a single band of 300 bp.

Zebrafish zgc:165502 gene expression during early embryogenesis. An antisense and sense riboprobe were generated to perform WISH for the stages that presented a 300 bp band in RT-PCR experiments results, as well as to determine the spatial temporal expression pattern of the folate receptor of those stages (Figures 17 and 18). All of the stages tested with the antisense probe demonstrated the presence of zgc:165502 mRNA, while sense probe assayed at the same stages were negative. The stages from the zygote period (1-cell) up to the late segmentation period (24 hpf) express the folate receptor globally (Figure 17). After 1dpf the expression pattern of the zgc:165502 gene becomes more localized and specific (Figure 18). By 2 dpf, the late pharyngula stage, zgc:165502 expression is seen in the head and heart of the embryo.

Most enzymes in the folate pathway that have been previously investigated in zebrafish were found to be maternally loaded and expressed throughout the early embryo.

Inhibition of these enzymes were lethal (Sun, *et al.*., 2009; Gross and Dowling, 2005; Kao, *et al.*., 2007). The results from this investigation support the findings of these studies, and suggest that during these periods the folate receptor is used to support cell division although not necessarily cell differentiation.

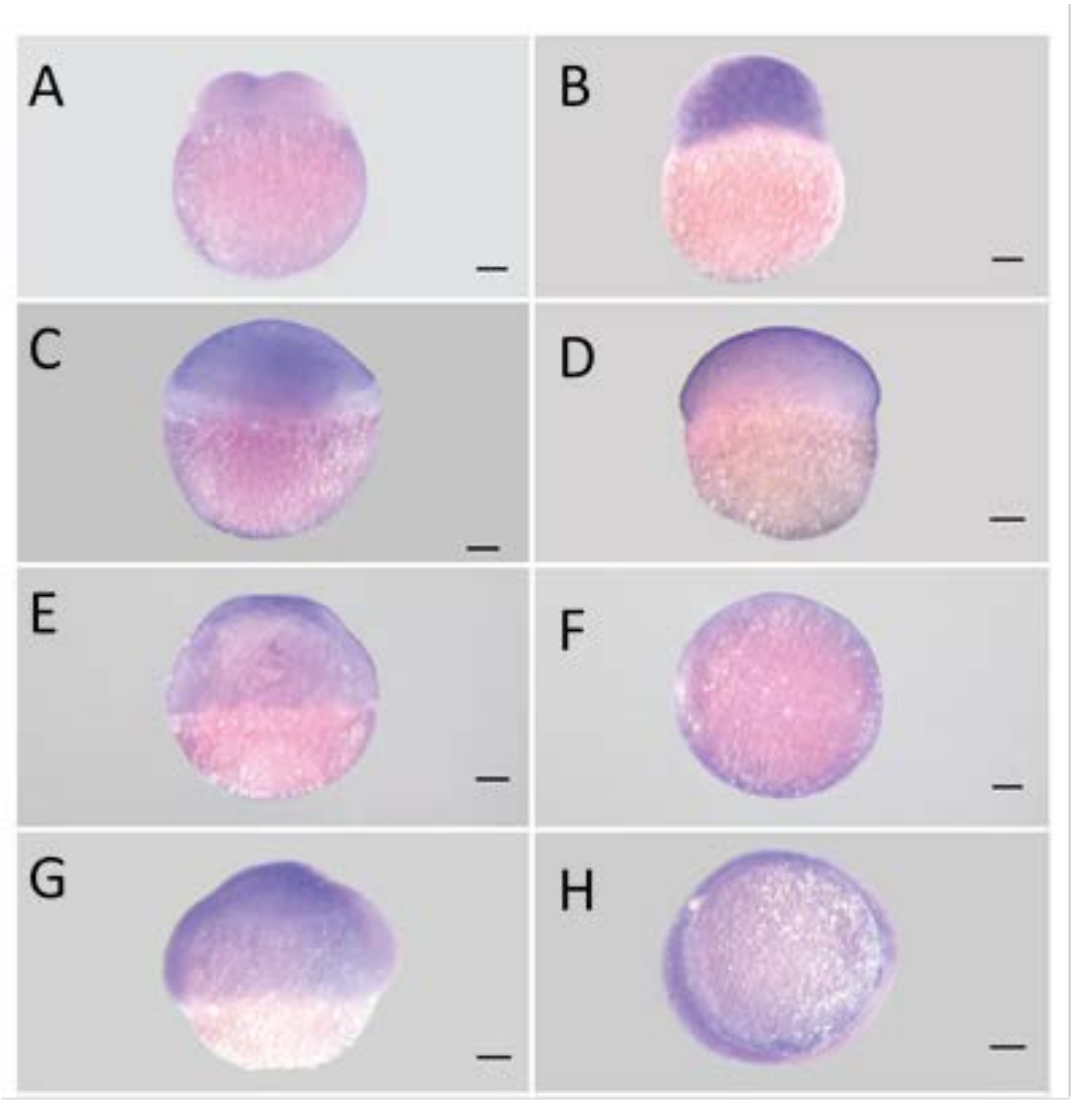

Figure 17. WISH Results for 1-2 Cell to Shield Stage. zgc:165502 is globally expressed (a) 1-2 cell (lateral), (b) 256 cell (lateral), (c) sphere (lateral), (d) 30% epiboly (lateral), (e) germ ring (lateral), (f) germ ring (top), (g) shield (lateral), (h) shield (top)

Figure 18. WISH Results for 1 dpf to 4 dpf. (a) 1 dpf is globally expressed (b)2 dpf expression is shown in the head (c) expression is shown in the pectoral and caudal fin (d) expression is shown in the cloaca and pectoral fin

It has been reported that dihydrofolate reductase (DHFR), an enzyme that plays a significant role in folate-mediated metabolism, also has a tissue specific expression and is abundantly expressed in the brains of zebrafish during early development (Sun, *et al.*., 2011). DHFR knockdown studies resulted in malformation of the heart (Sun, *et al.*., 2010). Other studies that treat embryos with methotrexate (MTX), a folate antagonist, showed that rescuing treated embryos with folate resulted in decreasing the cardiac deformities (Ma, *et al.*., 2012). Similarly, studies exposing zebrafish to selenite during early embryo development resulted in cardiac and neural defects, but these effects were prevented with folate administration (Muralidharon, *et al.*., 2015). Recently, folic acid supplementation has been shown to rescue retinal defects induced by ethanol exposure in zebrafish during retinal neurogenesis (1-2 dpf) (Parkin, *et al.*., 2009). The results of these various studies support the conclusion that folate is necessary for cell differentiation.

Furthermore, if folate is pivotal at these stages of development, the folate receptor will also be necessary and it should be expressed in corresponding regions, which this study has shown.

Zebrafish zgc:165502 gene expression during late embryogenesis. Once the embryo reaches the hatching period (2-3 dpf) and continues to the early larval stage (4 dpf), zgc:165502 expression is seen in specific tissues. The pectoral, dorsal, and caudal fins, which begin to develop around 36 hpf, start to show zgc:165502 expression by 2 dpf. Both development and expression continue through 4 dpf. The expression of zgc:165502 mRNA in the fins are consistent with previous studies in literature that inhibited DHFR. Using low concentrations of MTX, DHFR was inhibited prior to fin development and the embryo exhibited ventral edemas, dorsal curvature, and a shortened anterior-posterior axis, along with other defects at this stage (Sun, *et al.*., 2009). It is reasonable to infer from this that folate is essential for the growth and development of the fins.

Development of the digestive tract is initiated around 2 dpf and the gut tube development concludes around 4 dpf (Pyati, *et al.*., 2006) when the cloaca begins the final stages of development (Kalli, *et al.*., 2008). Expression of the zgc:165502 gene was detected in the digestive tract at 3 dpf and in the cloaca at 4 dpf. This indicates that the folate receptor is present at a time and place during development when folate could be needed to sustain the growth and development of the digestive organs, including the cloaca.

Fluorescent-tagged folate is selectively taken up during development. To further confirm the presence of the zgc:165502 protein 3 dpf embryos were treated with fluorescent-tagged folate. As a control, embryos were also exposed to the fluorescent dye, free of folate (RH). After 24 h of exposure, the embryos were washed with embryo media and observed for fluorescence (Figure 19). Living embryos treated with FA-BSA-RH demonstrated bright fluorescence in the head and cloaca, which is where we observed the presence of zgc:165502 mRNA by WISH. All embryos assayed, including controls, fluoresced in the gut. We hypothesized that this was due to the ingestion of the fluorescent compounds rather than the zgc:165502 protein being present. To test this hypothesis, embryos were placed in media free of fluorescent dyes and folate for 24 h after their initial exposure to fluorescent-tagged folate and then observed again. The control embryos did not show any residual fluorescence, while the embryos that were initially treated with fluorescent-tagged folate showed the same fluorescent profile seen previously. These results demonstrate the ability of tissues shown by *in situ* hybridization to have zgc:165502 mRNA also have the ability to internalize folate. We have shown for the first time, that tagged folate can be selectively taken up during embryo development in a targeted fashion.

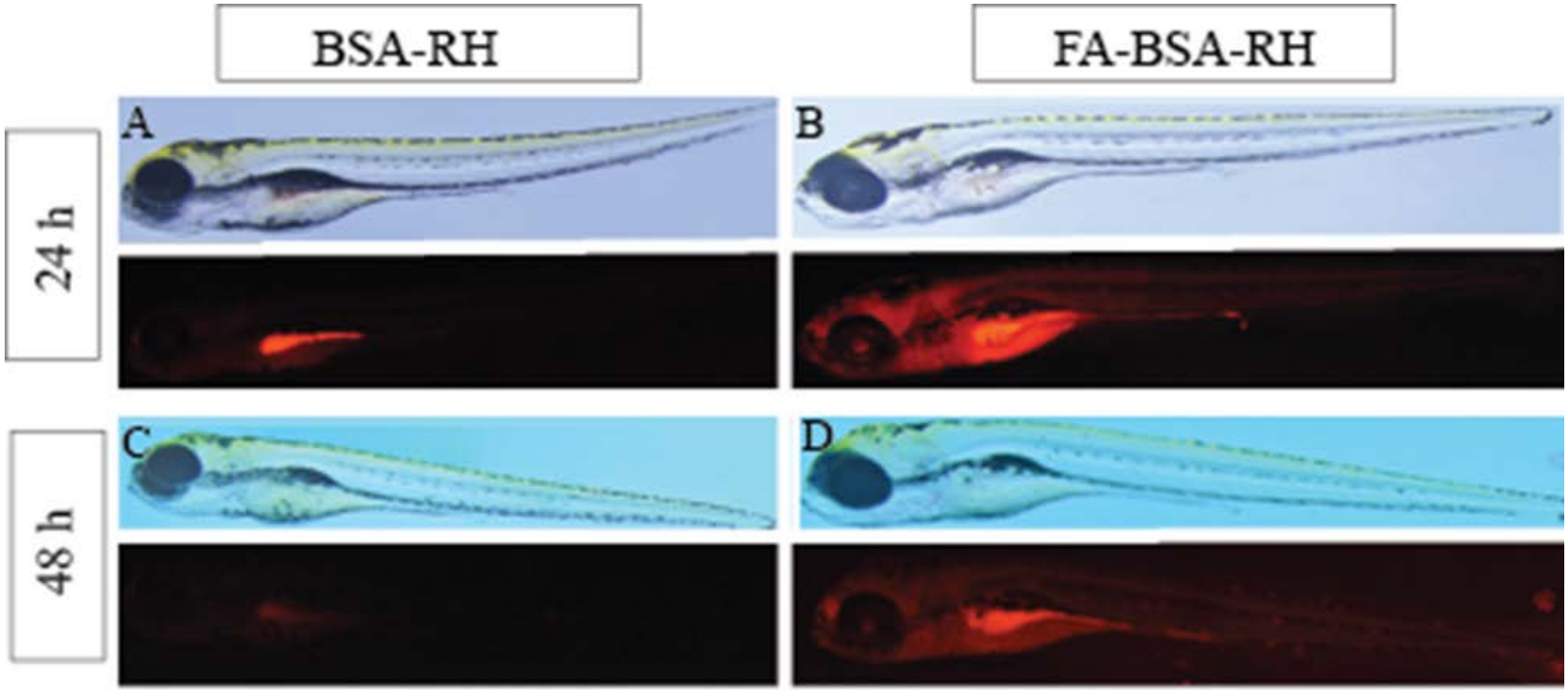

Figure 19. Fluorescent Tagged Folate Uptake. 3dpf staged embryos were treated with 50 µM of fluorescent tagged folate (FA-BSA-RH) and as a control embryos were also treated with non-folate fluorescent dye at the same concentration. After 24 h exposure to fluorescent dye (A) and fluorescent tagged folate (B) embryos displayed fluorescence. After an additional 24h in fluorescent dye (C) and fluorescent folate free media (D), only D exhibited fluorescence.

Conclusions

The folate receptor provides information as to when (developmentally) and where (spatially) folate can enter into the zebrafish. This study presents the gene expression pattern for the zebrafish zgc:165502 gene during embryogenesis. We have shown that the folate binding sites (FBS) in the FOLR1 protein in humans are conserved in zebrafish. In addition, we have elucidated the globally expression of the folate receptor mRNA in zebrafish during the first 24 hpf and the more specific, localized expression during late embryogenesis.

This information can aid in optimizing current treatments for folate specific diseases, as well as potentially provide an avenue for researchers to further investigate folate specific conditions such as neural tube defects.

Many cancers have an upregulated folate receptor (Sudimack and Lee, 2000), and targeting the receptor has proven to be a useful method to increase specificity and potency of drug treatments (Leamon and Reddy, 2004). The use of zebrafish and exploiting the folate receptor can help to advance the field of field of cancer research that targets the folate receptor. We have demonstrated the ability to exploit the folate receptor by use of fluorescent tagged folate.

CHAPTER FIVE

SELECTIVE TARGETTING OF CELLS IN ZEBRAFISH USING FOLATE MEDIATED PHOTODYNAMIC THERAPY AGENT

Introduction

The ability to selectively kill cells in a spatiotemporal fashion can provide insight into development. Many cancers overexpress the folate receptor (Bisland *et al.*, 1999) due to its role in the synthesis of nucleic acids and amino acids (Choi and Mason, 2000; Keleman, 2006). These cells can be selectively targeted by exploitation of the receptor. Many agents that specifically targets cancerous cells have been developed (Sudiamack and Lee, 2000; Leamon and Reddy, 2004; Lee and Low, 2012). These agents are taken up into the cell's cytoplasm via receptor mediated endocytosis (Sudiamack and Lee, 2000; Leamon and Reddy, 2004; Lee and Low, 2012). When folate (FA) is conjugated to a photosensitizer (PS), both the FA and the PS can be internalized into the cell (Lee and Low, 2012). Upon photoactivation the conjugate produces singlet oxygen which damages the cell and can lead to cell death. This method of effecting specific cells with PS that produces reactive oxygen species is called photodynamic therapy. Since embryonic cells also express folate receptors (as shown in Chapter Four) these PDT agents can be used to investigate early development.

A common PS that has been used in targeted and non-targeted studies is chlorin e6 (Ce6) agent that has FA and Ce6 covalently attached to bovine serum albumin,

FA-BSA-Ce6 (discussed in depth in Chapter Three) that is effective as a folate directed PDT agent in HeLa cell culture.

Selective cell targeting coupled with PDT has been studied in many organism, and through our search of the literature we believe zebrafish have yet to be used in these types of studies. Zebrafish are good candidates for these studies because they are vertebrates and they share a high degree of sequence and functional homology with humans, their embryos and larvae are transparent making it easy to see the impact of treatment with invasive techniques, and they produce a large number of offspring at one time (Kao, *et al.,* 2014).

We have previously elucidated the gene expression pattern for the folate receptor during zebrafish embryogenesis (discussed in Chapter Four). Here we report on the exploitation of the receptor by selective targeting of cells that express the folate receptor.

Materials and Methods

Reagents.1-ethyl-3-(3dimethylaminopropyl)carbodimide (EDC), bovine serum albumin (BSA), anhydrous dimethyl sulfoxide (DMSO), ethanolamine, folate (FA), N-hydroxysuccinimide (NHS), Rhodamine B isothiocyanate (RH), Acridine Orange (AO), were purchased from Sigma Chemical Company (St. Louis, MO). Chlorin e6 (Ce6) was purchased from Frontier Scientific (Logan, UT). All other chemicals used were analytical grade and used without further purification, unless otherwise specified.

Zebrafish care and husbandry. Zebrafish were maintained at Loyola University Chicago. All studies were performed with the approval of the Institutional Animal Care and Use Committee (IACUC). Wild-type embryos were raised and staged as described in

Kimmel *et al.*, 1995. Post-gastrulation stages were treated with 0.005% 1-phenyl-2-thiourea (PTU) solution to prevent melanin pigment from developing. Embryos older than 24 h post fertilization (hpf) were treated with fresh PTU solution once a day. Once the embryos reached the desired stage, they were dechorionated manually if necessary, anesthetized with 0.2% Tricaine pH 7.0, then fixed in 4% paraformaldehyde (PFA) in PBS pH 7.0 at 4°C. After fixing, the embryos were washed four times with phosphate buffered saline with 0.1% Tween-20 (PBST). After washing, the embryos were placed in 100% methanol (MeOH) and stored at −20 °C.

Synthesis and characterization of non-fluorescent folate targeted compounds. FA-BSA-Ce6 and BSA-Ce6 were synthesized and characterized as detailed in Chapter Three. The final products, BSA-Ce6 and FA-BSA-Ce6 were diluted to a final concentration of 5 µM and 10 µM using embryo media.

Selective cell targeting with FA-BSA-Ce6. Wild type zebrafish embryos were collected at 2 days post fertilization (dpf) and 3 dpf. Three embryos were placed in a single well that contained 3 mL of either 5 µM or 10 µM of BSA in embryo media, BSA-Ce6, or FA-BSA-Ce6. The wells were placed in a 37°C incubator overnight in the dark. After 24 h, the solutions were removed and the live embryos were washed 3X with embryo media and returned to the incubator overnight. The following day each embryo was irradiated with light at 660 nm for 1 min, 2 min, 4 min, and 6 min which corresponds to 5.6, 11.2, 22.5, and 33.7 J/cm^2 respectively. Each embryo was determined to be viable or non-viable based on response to touch and heartbeat. A total of 24 live embryos were assayed with each conjugate.

Confirmation of selective cell targeting. After the embryos were treated with PDT agents as described, they were immersed in 5 μg/ml Acridine Orange (AO) for 10 min. Following treatment with AO each embryo was imaged for less than 60 s using a stereo fluorescent microscope with FITC filter.

Results

Synthesis of conjugates. We have synthesized FA-BSA-Ce6 and BSA-Ce6 as previously described in Chapter Three. Briefly, a 10 molar excess of FA that was previoulsy esterified using a water soluable carbodiimide was covalently attached to BSA via amidation, producing FA-BSA. BSA-Ce6 was produced in th same manner, except Ce6 was used in a 20 fold molar excess to BSA. To generate FA-BSA-Ce6, Ce6 was covalently attached to FA-BSA, by the same esterification and proceeding amidation reaction. The final conjugates, BSA-Ce6 and FA-BSA-Ce6 were dialyzed in phosphate buffered saline pH 7.4. Based on UV-Vis absorption spectroscopy it was deteremined that each sample produced contained 8 covalently attached Ce6 to BSA, and 2 molecules of FA.

FA-BSA-Ce6 effectiveness in zebrafish. All embryos treated with BSA-Ce6, BSA, and embryo media that were assayed under all conditions discussed were determined to be viable for up to 24 h after light exposure. All embryos that were kept in the dark remained viable for up to 72 h after immersion in conjugates. Embryos exposed to 1 and 2.5 μM FA-BSA-Ce6 were determined to be viable based on reaction to stimulus and continued heartbeat for up to 24 h after light exposure.

The results of FA-BSA-Ce6 at 5 and 10 µM on 4 dpf staged embryos (48 h after 2 dpf embryos were treated with conjugates) are shown in Table 3. Embryos exposed to 1 min and 2 min of light were all deemed viable. The embryos exposed to FA-BSA-Ce6 at both concentrations were non-viable at the end of 4 min and 6 min light exposure.

Light exposure time	**5 uM**	**10 uM**
1min	0	0
2 min	0	0
4 min	24	24
6 min	24	24

Table 3. Non-viable embryos after PDT treatment. Results of FA-BSA-Ce6 at 5 and 10 µM on 4 dpf staged embryos. Embryos exposed to light greater than 4 min were all non-viable, embryos exposed to light under 4 min were all viable after PDT treatment.

To determine how much light was needed to induce death the trials were video recorded. Viability was based on heart beat; once the heart beat could no longer be detected the embryo was deemed non-viable. For 5 µM FA-BSA-Ce6 the embryos were non-viable on average after 3:42 minu (222 seconds) of continuous light exposure. For 10 µM FA-BSA-Ce6 the heart beat stopped on average after 3:20 minutes (200 seconds) of continuous light exposure.

The results for trials carried out using 5 dpf (48 h after 3 dpf embryos were treated with conjugates) were also video recorded. Each trial was video recorded from the onset of light irradiation. For both 5 and 10 µM FA-BSA-Ce6, the embryos were reactive and visually appeared to be unaffected for light exposure under 3 min. Beginning around 3 min of light irradiation, 5 dpf embryos began to tremor. Of the 36 embryos treated with 5 µM FA-BSA-Ce6, all 36 began to tremor and 12 were unreactive to stimulus (did not move when touched). 36 embryos were treated with 10 µM FA-BSA-Ce6 and all began to tremor beginning at 3 min of light irradiation and were unreactive to stimulus, unlike the 5 µM samples. All embryos regained "normal" functions (based on heart beat, reaction to touch, phenotype) after 24 h of irradiation.

Selective targeting of cells. To visualize cells that were effected by photodynamic therapy treatment with 5 and 10 µM FA-BSA-Ce6 we carried out cell death assay with acridine orange. The results of trials with 10 µM FA-BSA-Ce6 are presented in Figure 19. As a control we treated embryos staged at 5 dpf in embryo media. 5 & 10 µM FA-BSA-Ce6 embryos show significant cell death over control. There appears to be no significant difference between 5 & 10 µM FA-BSA-Ce6. 36 embryos were assayed, 4 died while determining correct acridine orange concentration. The other 32 exhibited the same fluorescence pattern.

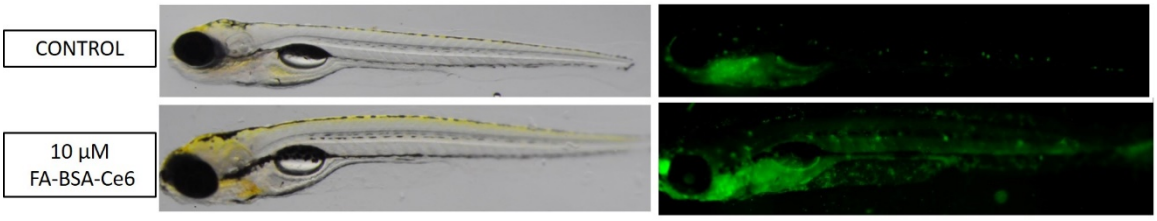

Figure 20. Acridine Orange Assay Results. 5 dpf Embryos treated with FA-BSA-Ce6 showed significant cell death over embryo media control. There was no observable difference between 5 and 10 µM samples. Image presented is indicative of both concentrations.

Conclusions

Leamon and colleagues (Leamon, et. al, 1993) and many others have shown that the folate receptor in cell culture can be exploited with folate conjugated macromolecules. We hypothesized that by attaching FA to our BSA-Ce6 carrier molecule, the conjugate will be taken up by receptor mediated endocytosis. Previous work in our laboratory has proven that not only does zebrafish express the folate receptor during embryogenesis (shown in Chapter Four), but they can also take up a FA bound to a macromolecule via receptor mediated endocytosis (Chapter Four). In this study we synthesized an analog of the fluorescent compound produced in prior studies presented in Chapter Three. We replaced the fluorescent dye with a photoactive dye, Ce6. Ce6 is known for its large quantum yield of singlet oxygen produced via photodynamic action. In this study we set out to exploit the folate receptor in zebrafish to selectively target and effect cells that express the folate receptor.

Photodynamic treatment trials were carried out on zebrafish embryos. To ensure that the results produced by the light trials were due to the photodynamic action of the targeted compounds we carried out these trials in the dark. All embryos exposed to FA-BSA-Ce6, BSA-Ce6, BSA, and embryo media were viable up to 48 h after exposure. The same cannot be said for embryos treated FA-BSA-Ce6 that were irradiated with light. From this we can conclude that the results we received from light based studies were due to phototoxicity of the conjugates. These results support the results presented in Chapter Three, where over 96% of HeLa cells survived after being exposed to the conjugates in the dark, yet there was significant cell death upon photoactivation.

Photodynamic treatment of 4 and 5 dpf with our targeted agents resulted in all embryos treated with lower concentrations, 1 and 2.5 μM FA-BSA-Ce6, and BSA-Ce6, remained viable after treatment with up to 6 min of light. In addition, all embryos that were exposed to controls survived as well as embryos exposed to the conjugates but not irradiated with light survived. This was to be expected, because based on our results from the cell culture trials, where 26% of cells were non-viable after treatment with 2 μM FA-BSA-Ce6, and less than 2% of cells were non-viable for cells kept in the dark. Therefore, we concluded that our conjugates are not cytotoxic in the dark, and 1 and 2.5 μM FA-BSA-Ce6 combined with 6 min of light does not produce significant cell death.

All embryos survived light treatment with 5 and 10 μM BSA-Ce6 and BSA. 4 and 5 dpf embryos that were treated with 5 and 10 μM FA-BSA-Ce6 survived treatment with 1 and 2 min of light. 4 dpf embryo treated at this same concentration but higher light dosage, 4 and 6 min, did not survive, yet, 5 dpf embryos treated at these same

concentrations remained viable, but treatment induce tremors after 3 min of light exposure. The embryos were checked 24 h after the induction of tremors and all signs of this effect were absent. To further investigate, those same embryos were exposed to light again. This second exposure did not induce tremors or any other noticeable effects. When checked for cell death, these embryos exhibited enhanced cell death over controls. Based on these results we concluded that our targeted PDT agent effects specific cells, not all cells.

Discussion

Folate is a B vitamin that plays a significant role in the prevention of neural tube defects (NTDs) and homocysteinemia (Barnabe, *et al.*, 2015; Williams, et. al, 2015; Mills, *et al.*, 1995; Rosenquist, *et al.*, 1996). NTDs are malformations of the brain and spinal cord that occurs during gestation (Botto, *et al.*, 1999; Lemuire, 1988). Folate is needed for the methylation of homocysteine to form methionine and the synthesis of deoxynucleotides needed for DNA replication (Kang, *et al.*, 1987; Krishnaswamy and Nair, 2001). Increased levels of homocysteine (homocysteinemia) are suspected to play important roles in developmental defects and is a risk factor for ischemic heart disease (Krishnaswamy and Nair, 2001; Wald, *et al.*, 1998). NTDs and the effects of homocysteine have been documented in zebrafish (Blair, *et al.*, 2005; Muralidharon, *et al.*, 2015; Parkin, *et al.*, 2006). These studies show that inhibition of enzymes that metabolize folate increased the occurrence of these conditions, and supplementation with folate decreased their occurrence.

This study shows that cells that express the folate receptor can be selectively targeted and manipulated over cells that do not express the receptor. Photodynamic treatment with 5 dpf resulted in the embryo remaining viable, yet tremors were induced. The results from the acridine orange assay demonstrates that we effected selected cells. This discovery can lead to further investigation of folate specific diseases and cancers, in addition to helping to understand embryonic development.

CHAPTER SIX

CONCLUSIONS

Photodynamic therapy (PDT) utilizes oxidative damage to kill cancerous cells. Light excites a photosensitizer (PS), which then reacts with oxygen to form a highly reactive oxygen species, which includes singlet oxygen. This singlet oxygen reacts with cellular macromolecules to cause lethal damage. A prevalent concern with current FDA-approved PDT drugs is that they exhibit low selectively for cancerous cells over healthy cells. An approach to enhance selectively is to covalently attach a targeting moiety to a PS. Many cancers overexpress the folate receptor (Zwicke 2012; Parker 2005), therefore generating an agent that selectively targets that receptor is beneficial. The main objective of this research was to synthesize and characterize the folate directed, protein based photodynamic therapy agent, FA-BSA-Ce6. In addition, we wanted to show its effectiveness as a selective cell targeting agent in cell culture and *in vivo*.

The PS used in our conjugate was chlorin e6 (Ce6). Ce6 is a useful PS due to its absorbance in the optimum therapeutic window and high quantum yield of singlet oxygen. In addition, Ce6 has three carboxyl groups that provides sites for straightforward conjugation to other molecules that contain primary amines. A major drawback to Ce6 is its tendency to aggregate in aqueous environments. To overcome this disadvantage, we

conjugated Ce6 to the protein, bovine serum albumin (BSA) through an amidation reaction with the lysine residues on BSA.

BSA served as a scaffold to which multiple molecules of Ce6 could be attached due to its high number of lysine residues. Although BSA has 60 lysine residues, Huang and Kim showed that only 34 of those residues could be modified via lysine specific crosslinkers and those lysines were between 20-24 Å apart. We hypothesize that due to steric hindrance we were able to attached 10 molecules of Ce6 and two molecules of FA onto one molecule of BSA despite using ratios of Ce6:BSA as high as 30:1 and FA:BSA as high as 10:1.

An effective PDT agent will be phototoxic upon irradiation with light at the appropriate wavelength, but not cytotoxic in the absence of light. By using the singlet oxygen sensor, ρ-nitroso-N,N'-dimethylaniline (RNO), we were able to confirm that singlet oxygen was produced upon photoactivation of FA-BSA-Ce6 with 660 nm light and that singlet oxygen was not produce in the absence of light *in vitro*. In HeLa cell culture, cells that were exposed to FA-BSA-Ce6 varying in concentration from 1-10 μM that were kept in the dark resulted in 93% or greater cell survival. Cell survival decreased significantly, to as low as 5% upon photoactivation. *In vivo* studies with zebrafish embryos that were exposed to 5 and 10 μM FA-BSA-Ce6 but kept in the dark resulted in all embryos remaining viable for at least 48 h after exposure and none of the embryos remained viable after photoactivation with light times greater than 3 mins. Results from these *in vitro* and *in vivo* studies showed that FA-BSA-Ce6 is not cytotoxic in dark but it is phototoxic upon irradiation at 660 nm.

As shown in Figure 12 HeLa cell survival is both concentration and light dose dependent. As the concentration of FA-BSA-Ce6 increase and as light exposure time increases (thus irradiation energy increases), cell survival decreases. The same effects are not seen with BSA-Ce6 (Figure 11). In fact, cell survival across all light irradiation times remained above 92% for BSA-Ce6. In zebrafish trials, the trend continued. Embryos exposed to BSA-Ce6 remained viable upon photoactivation. We synthesized a fluorescent analog of FA-BSA-Ce6 that contained FA-BSA, but Ce6 was replaced with Rhodamine B (RH), due to Ce6 poor fluorescence. Zebrafish embryos were treated with BSA-RH or FA-BSA-RH. After allowing time for the embryo's gut to empty, embryos treated with BSA-RH showed little to no fluorescence. Embryos treated with the FA-BSA-RH brightly fluoresced. Additionally, the gene expression pattern for the folate receptor during zerbrafish early development was elucidated. Embryos treated with FA-BSA-RH exhibited fluorescence in the same pattern that was shown via whole mount *in situ* hybridization (WISH). From the fluorescence data using FA-BSA-RH, the WISH data, the high cell survival after treatment with BSA-Ce6 and light, and the low cell survival from treatment with FA-BSA-Ce6 under the same conditions, it is highly suggestible that the conjugate is folate directed, and possibly being taken up via receptor mediated endocytosis.

Photodynamic treatment using FA-BSA-Ce6 with embryos staged at 5 days post fertilization (dpf), induced tremoring, although the embryos remained viable. Acridine orange experiments showed that cell death was occurring after treatment, and many of those cells exhibited florescence with treatment with FA-BSA-RH, and those cells showed the presence of the folate receptor in WISH experiments. This shows that FA-BSA-Ce6

can selectively target cells that express the folate receptor. The synthesis of FA-BSA-Ce6 coupled with being able to selectively target and effect folate dependent cells in zebrafish opens up many new opportunities for investigation. Zebrafish share a high homology similarity to humans therefore they are good candidates as *in vivo* models to look into folate specific diseases as well as cancers. The folate targeted PDT agent could also be used to aid in understanding embryonic development. Research has shown that folate may play a role in alzheimer's disease, nueral tube defects, cancers, cardiac diseases, and other neurological conditions (Botez and Reynolds, 1979; Clarke, *et al.* 1998; Reynolds, 2002; Seshadri, 2001). By using a folate directed agent, these diseases can be further examined and understood.

Besides knowing that FA-BSA-Ce6 produces singlet oxygen and singlet oxygen is toxic to cells, the actual mode or pathway to cell death is not well understood. It is not clear at what point during irradiation is singlet oxygen being produce. The studies discussed in this dissertation were end point analysis studies. It would be beneficial for studies to be carried out that monitor the production of singlet oxygen. This can be accomplished by in assay ROS detectors.

Depending on the stage of zebrafish embryo, results from photodynamic treatment varied. Younger staged embryos died, while older staged embryos survived but began to tremor. Studies that look into what particular cells are being effected *in vivo* can provide deeper insight. Investigations into an optimum conjugate exposure time, along with elucidating the cascading events that occur after treatment with FA-BSA-Ce6 can and should be further explored in both cell culture and *in vivo*. Those studies will provide

insight into how the cell responds to the treatment prior to cell death and can lead to more efficient and optimized conjugates.

FA-BSA-Ce6 provided cell death in both HeLa cell culture and in zebrafish embryos. Available molecular oxygen is a big contributor to the effectiveness of PDT. Cancer tumors tend to be hypoxic. Therefore, if a PDT agent is able to not only selectively target the cancerous cell, but also bring with it molecular oxygen, the effects of the PDT agent can be increased. Research in our laboratory has shown that a nanoparticle of up to 8 modified hemoglobin molecules can be synthesized, and this nanoparticle has a high affinity for oxygen (Webster, 2016 in press). Therefore, synthesizing an analog of FA-BSA-Ce6, by replacing BSA with the modified hemoglobin, can potentially deliver up to 10 molecules of Ce6, along with 8 molecules of hemoglobin can be beneficial. Each molecule of hemoglobin will potentially carry a molecule of oxygen inside the tumor, thereby increasing the availability of molecular oxygen, thus increasing the generation of singlet oxygen.

FA-BSA-RH was able to selectively target cells that express the folate receptor. Therefore, this analog can potentially be used for tumor imaging before and/or after treatment. Many cancers are treated from multiple approaches. Being able to have the tumor fluoresce can optimize surgical removal of tumors. In addition, provide a way to visualize how much of the tumor remains after surgery or after other cancer related treatments.

APPENDIX A

HEMOGLOBIN BASED PDT AGENTS

PDT potency has a direct relationship with oxygen availability. Cancerous cells are typically hypoxic due to the aggregation of cells, which prevents an appropriate vascular system from being developed. Hence, the more oxygen available to the photosensitizer the more cellular damage can be done. Crosslinked hemoglobin (XLHb) has been shown to have an increased oxygen affinity. Therefore, conjugating Ce6 to XLHb should allow for more molecular oxygen to be present inside the targeted cells, and result in increased cellular death.

We successfully synthesized 60 μM XLHb, FA-XLHb, and FA-XLHb-Ce6. The conjugates were extracted using cold acid/acetone mixture to quantify the amount of folates and chlorin e6 molecules covalently bound to the protein as described in Chapter Three. Under these harsh conditions, the heme dissociates from the globin, and the globin precipitates along with any covalently bound molecules. FA-XLHb-Ce6 proved to have approximately 2.67 folates and 3 chlorin e6 molecules bound per protein molecule (Table 4).

.

Trials	# of FA	# of Ce6
1	3	3
2	2	3
3	3	3

Table 4. Acid/Acetone Extraction. Average of 2.67 folates, and 3 chlorin e6 molecules bounds per XLHb molecule

A key component to successful PDT is providing sufficient oxygen that can be converted into singlet oxygen. The FA-XLHb-Ce6 conjugate was assayed for its oxygen affinity. An oxygen binding curve was collected (Figure 21) and a Hill plot was constructed to determine the conjugate's p50 (Figure 22). The p50 is the pO_2 at which the hemoglobin becomes 50% saturated with oxygen. As the p50 decreases, oxygen affinity increases. Unmodified hemoglobin has a p50 of approximately 26.5 mmHg. The p50 for the crosslinked hemoglobin that was used to synthesize FA-XLHb-Ce6 was determined to be 10.72 mmHg (+/- .245). The p50 for FA-XLHb-Ce6 was determined to be 7.98 mmHg (+/- .215) (Figure 21 and Table 5).

From Hill plots a Hill coefficient, "n", can be calculated. The Hill coefficient is a measure of cooperativity. Cooperativity is a measure of affinity for a ligand, and in our case an oxygen molecule, to bind to a substrate (crosslinked hemoglobin) upon the binding of another ligand at a different binding site. A Hill coefficient that is greater than one denotes positive cooperativity. The Hill coefficient for XLHb was determined to be 1.03 (+/- .010) and for FA-XLHb-Ce6 it was determined to be 1.70 (+/- .682) (Table 5 and Figure 22). This data demonstrates that upon conjugating XLHb to folate and chlorin e6 its oxygen affinity was enhanced. These results indicated that FA-XLHb-Ce6 oxygen affinity is greater than myoglobin (2.5 mmHg), yet lesser than Hb. Therefore, FA-XLHb-Ce6 should be able to hold on to oxygen in normoxic conditions, and deliver its oxygen in hypoxic conditions, such as in cancerous tumors.

Sample	P50	n
XLHb	10.72 (+/- .245)	1.03 (+/- .010)
FA-XLHb-Ce6	7.98 (+/- .215)	1.70 (+/- .682)

Table 5. P50 and Hill Coefficients. Data table of calculated p50 and hill coefficient for XLHb abd FA-XLHb-Ce6

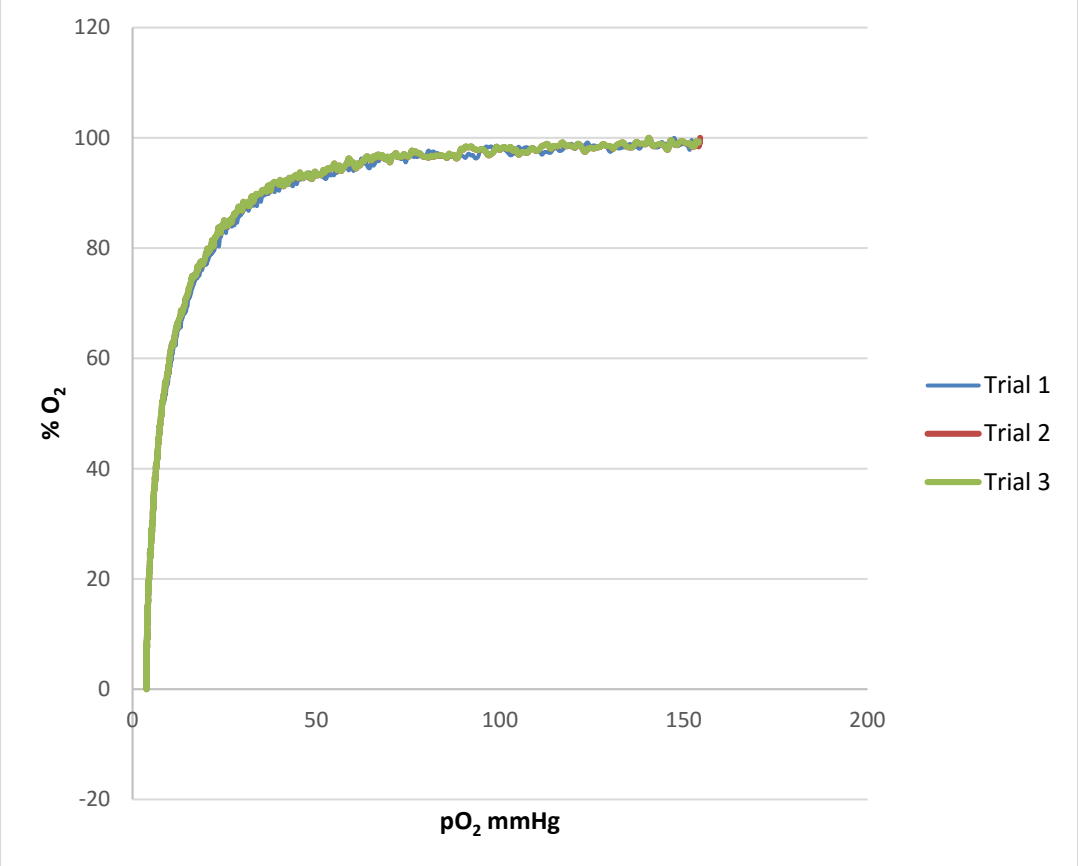

Figure 21. Oxygen Binding Curves for FA-XLHb-Ce6.

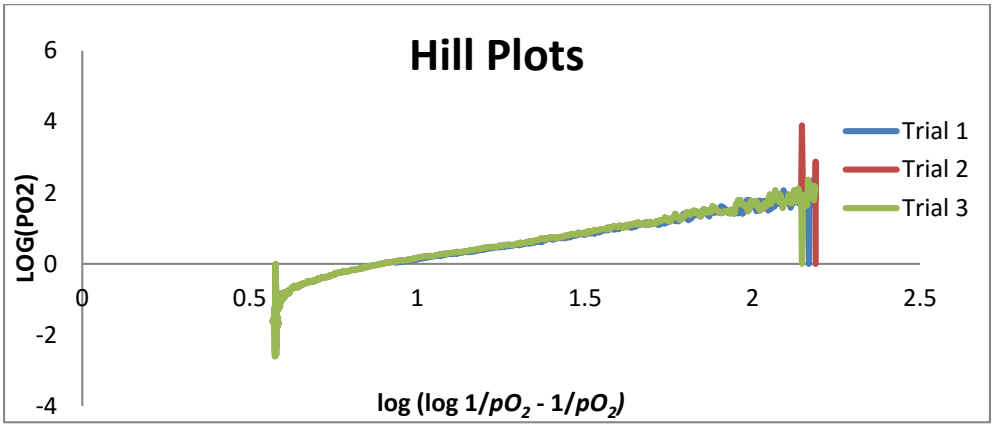

Figure 22. Hill Plots Calculated from Oxygen Binding Curves

Each conjugate was subsequently assayed for phototoxicity and dark cytotoxicity in HeLa cell culture using a 96 well plate and Cell Titer Blue Assay as previously described in Chapter Three.

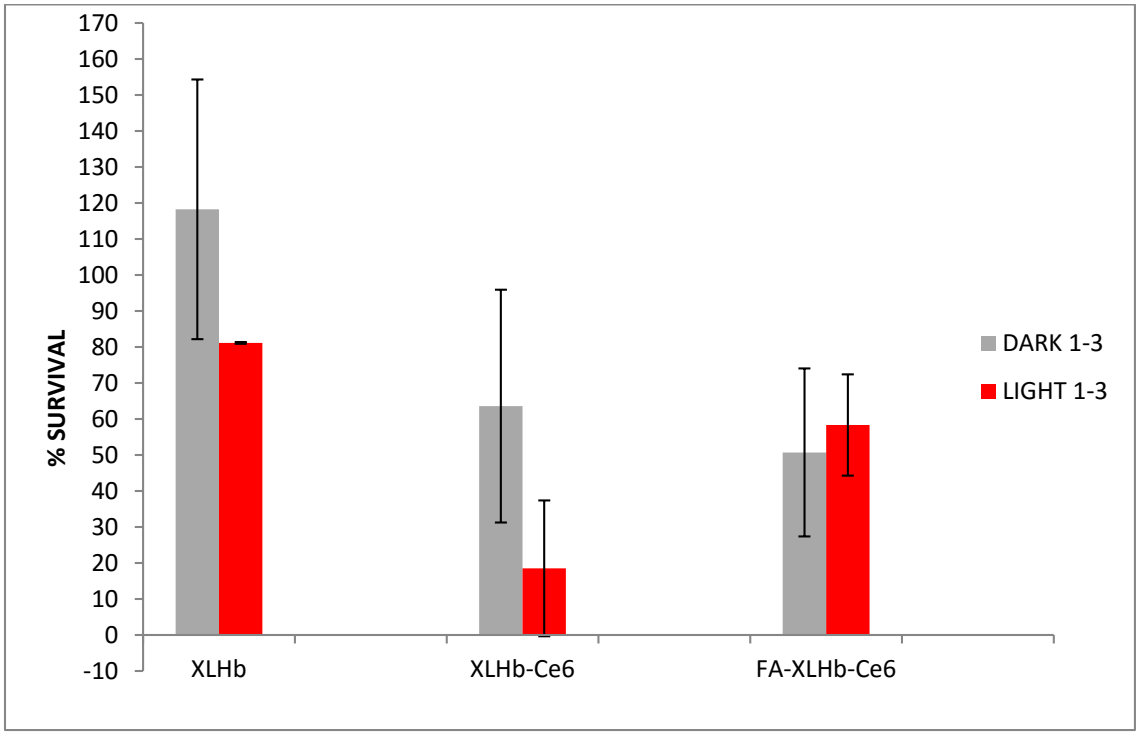

Figure 23. XLHb Based Conjugates Cell Culture Results.

The crosslinked hemoglobin compounds were shown to be cytotoxic. Crosslinked hemoglobin provided 118.22% cell survival, while the XLHb-Ce6 and FA-XLHb-Ce6 provided 63.57% and 50.69% cell survival, respectively. Phototoxicity results were 81.13%, 18.52%, and 58.32% for XLHb, XLHb-Ce6, FA-XL-Ce6 respectively (Figure 23). These results do not support our hypotheses. After further examination of the hemoglobin based conjugates, we determined that the hemoglobin had oxidized to become methemoglobin. Methemoglobin contains Fe^{3+}. This oxidized form of hemoglobin has a lower capacity to bind oxygen in comparison to unoxidized hemoglobin. Conversely, Fe^{3+} has a higher affinity for bound oxygen. When oxygen binds to methemoglobin the remaining Fe^{2+} of the tetramer have an increased affinity of oxygen. This results in the methemoglobin poorly delivering oxygen to tissues, causing hypoxia, which is lethal to cells. The samples were placed onto a dithionite reduction column, and results were not improved. The conjugates were successfully reduced, but after 24 h of incubation in a humidified atmosphere we hypothesize that the conjugates returned to the met-form.

The results obtained using a significant lesser amount of conjugates (10 μM) of BSA based conjugates provided more consistent (based on standard deviations) data and proved to be a more effective conjugate. It should be noted that the amount of light energy used was in these XLHb studies was 81 $mJ/cm^2/nm$ while the BSA studies were carried out with 168 $J/cm^2/nm$.

Brief Methods

Synthesis of XLHb. Prior to crosslinking hemoglobin at the β82-Lys residues, HbA was dialyzed in MOPS buffer at pH 7.0. The HbA was then reacted with bis-(3,5 dibromosalicyl) fumarate (DBSF) at a 1:1.1 molar ratio. Subsequently, it was incubated for 2h at 37 °C. The reaction was terminated on ice and reaction mixutre was dialyzed in .01 M Tris buffer at pH 8.5 overnight. The crosslinked hemoglobin was separated from umodified hemoglobin using a Sephadex A-50 column with a pH gradient of 8.5-7.0. XLHb was confirmed by SDS PAGE-gel electrophroesis.

Synthesis of FA-XLHb. Folic acid was placed inside of a small eppendorf tube covered with foil and dissolved in 200-300µl of dry DMSO. Next, it was incubated with a 10 fold molar excess of 1-ethyl-3-(3-dimehtylaminopropyl) carbodimide(EDC) and a 20 fold molar excess of N-hydroxysuccinimide (NHS) at room temperature for 30min. A 10 fold molar excess of the esterified “acitivated” folic acid per XLHb tetramer was added to the XLHb solution that was previously dialyzed in bicarbonate buffer at pH 8.0 The mixture was incubated for 24h at room temperature and quenched with ethanolamine. The excess folic acid, NHS and ethanolamine was removed by dialyzing overnight in PBS at pH 7.4.If the FA-XLHb were to be added to chlorin e6 it was dialyzed in bicarbonate buffer at pH 8.0.

Synthesis of XLHb-Ce6. Chlorin e6 was placed inside of a small eppendorf tube and covered with foil and dissolved in 200-300µl of dry DMSO. Next, it was incubated with a 10 fold molar excess of 1-ethyl-3-(3-dimehtylaminopropyl) carbodimide(EDC) and a 20 fold molar excess of N-hydroxysuccinimide at room temperature for 30min. A

10 fold molar excess of the esterified “acitivated” chlorin e6 per XLHb tetramer was added to XLHb that was previously dialyzed in bicarbonate buffer at pH 8.0 The mixture was incubated for 24h at room temperature and quenched with ethanolamine. The excess chlorin e6, NHS and ethanolamine was removed by dialyzing overnight in PBS at pH 7.4.

Synthesis of FA-XLHb-Ce6. Chlorin e6 was placed inside of a small eppendorf tube and covered with foil and dissolved in 200-300µl of dry DMSO. Next, it was incubated with a 10 fold molar excess of 1-ethyl-3-(3-dimehtylaminopropyl) carbodimide (EDC) and a 20 fold molar excess of N-hydroxysuccinimide (NHS) at room temperature for 30min. A 10 fold molar excess of the esterified “acitivated” chlorin e6 per XLHb tetramer was added to the FA-XLHb solution that was previously dialyzed in bicarbonate buffer at pH 8.0 The mixture was incubated for 24h at room temperature and quenched with ethanolamine. The excess chlorin e6, NHS and ethanolamine was removed by dialyzing overnight in PBS at ph 7.4.

Oxygen binding. Four milliliters XLHb or FA-XLHb-Ce6 in MOPS buffer pH 7.0 was placed inside of the Hemox Analayzer Model B. The sample was allowed to equilibrate until it has reached 37°C (approximately 30min). The XLHb is oxygenated with air supplied from an air tank. After the XLHb has been completely oxygenated and the pO_2 has been adjusted to 150mmHg, the sample is deoxygenated by switching off the air and turning on the nitrogen. The completion of the curve is reached when the pO_2 approaches zero.

APPENDIX B

PEG BASED PDT AGENTS

A PEG based conjugate was synthesized in addition to the protein based conjugates. The amines on the PEG allowed for the same carbodiimide esterification chemistry to be used for conjugation of folate and dye that was used with the protein based conjugates. It also helped maintain solubility. The 4 arm-amine PEG (CreativePEGworks, Winston Salem, NC 27113) (Figure 24), was placed inside of a vial covered with foil. A fifty fold molar excess of chlorin e6, 50 fold molar excess of 1-hydroxybenzotriazole, 17 fold molar excess of folic acid, 50 fold molar excess of EDC was added to the vial and they were dissolved with 3-5mL of dry DMF. Once all reagents were dissolved a 50 fold molar excess of triethylamine was addition to the mixture and the vial was placed on a stir plate at 4°C. The resulting mixture was separated using gel filtration, and the number of molecules bound was determined via UV-Vis spectrophotometry for each fraction collected. Chlorin e6 has maxima absorption at 660 nm, and folate has maxima absorption at 363 nm. The absorbances at 363 nm was corrected for slight overlapping absorption of chlorin e6 and the ratio of dye to folate was calculated (Table 6). It was determined that fraction two contained the desired the ratio, 3:1, and was subsequently used in two HeLa Cell Culture trials. The results of the two trials indicated that the 19% and 48% of cells survived respectively after irradiation with light. In the dark the conjugates showed 54% cell survival. Therefore, the conjugate was deemed cytotoxic. It should be noted that the unlike the protein based conjugates cell survival was assayed using MTT and not Cell Titer Blue.

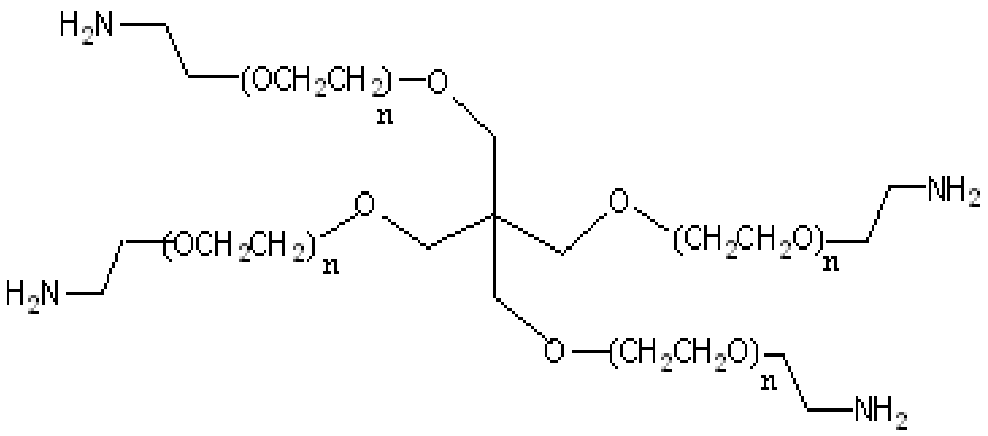

Figure 24. 4-Arm Amine PEG.

Fraction	Ratio (Ce6:FA)
1	7.88
2	3.09
3	3.89
4	3.36
5	2.56
6	4.28
7	4.74
8	3.96

Table 6. Ratio of Ce6:FA Bound to 4-Arm Amine PEG. Fraction separated and collected via gel filtration using a G-10 Sephadex column. An UV-vis spectrum was taken of each fraction and subsequently ratios were determined

APPENDIX C

LAMP STUDIES

To determine the exact energy output of the lamp, its energy was measured against a calibrated light source. These experiments were carried out with the assistance of Dr. Robert Polak in the Physics Department at Loyola University Chicago. The experiment was briefly explained by Dr. Polak in an email sent to RoJenia Jones on August 12, 2014. The text from the email is below:

"The total power emitted in electromagnetic waves for a light source is called the radiant flux and is measured in units of Watts (W). The power emitted by the light source for an electromagnetic wave at a specific wavelength is called spectral radiant flux and is typically measured in (W/nm).
To determine the spectral radiant flux of an object, we compare the light being emitted by it at a specific wavelength to that being generated by a calibrated light source. In this case, we have a calibrated light from Labsphere, which consists of a 2π ("two-pi") incandescent light source being driven by a calibrated power supply. This light enters an integrating sphere and the detector used is an opal glass. By comparing the light energy on the detector to that of an unknown source at a specific wavelength, we can then determine the spectral radiant flux of the unknown source.
The opal glass itself is not a detector though. Instead we use a Topcon SR-3 Photoradiometer to determine the spectral radiance (light energy per unit area per unit solid angle) on the surface of the opal glass. The spectral radiant flux of the unknown source can then be determined by:
the spectral radiant flux of the unknown source, is the spectral radiant flux of the calibrated light source (data provided by Labview), *is the spectral radiance of the opal glass with the unknown source and is the spectral radiance of the opal glass with the calibrated light source.*
In this case, we actually aren't interested in the spectral radiant flux of the unknown light source, but the light power per unit area per unit wavelength where the cultures are placed. This is the spectral irradiance and is simply the spectral radiant flux of the light entering the integrating sphere through an open port divided by the area of that port.
To determine this, the light source was placed 3 inches from the port opening and moved to measure the light entering the sphere that would correspond to different positions of the culture. We broke this into 12 different bins (each representing a different area of the culture tray). Using the above formula to determine the spectral radiant flux incident upon each bin, we can then determine the spectral irradiance by dividing this result by the area of the port opening"

All measurements were taken with the source 16 inches from the tray. The irradiance will go as $1/r^2$ from the source, so changing the distance from 16 inches to 18

inches will result in a 21% decrease in the irradiance. There were three trials completed for each lamp source tested. Below is a diagram of each “bin”:

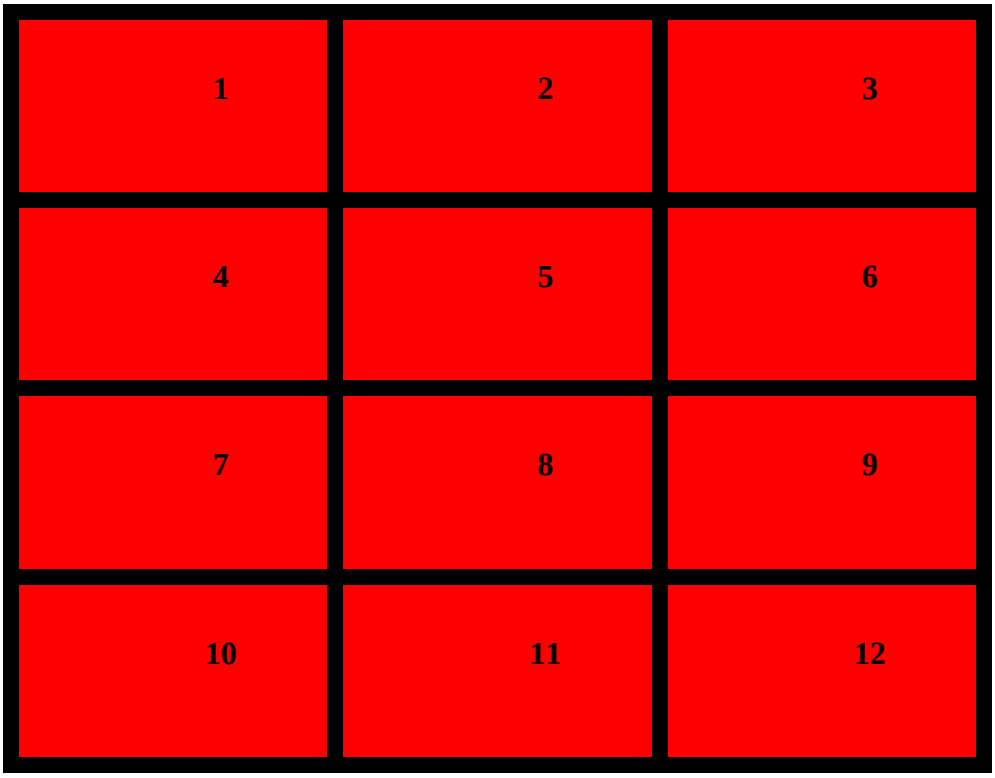

Figure 25. Lamp Bins

All data reported in this dissertation (unless otherwise stated) was carried out with a 120 red LED lamp (660 nm) purchased from Elixa (http://www.elixa.com/shop/120-led-red-660nm/). The LED array is approximately 3/4″x 2″x 4″. The results from the light intensity study for wavelengths 380 – 780 nm is presented in Figure 26.

In Table 7 and Figure 27, the data is presented for the amount of energy produced at 660 nm with the lamp 3 inches away from the test surface for 1-10 min.

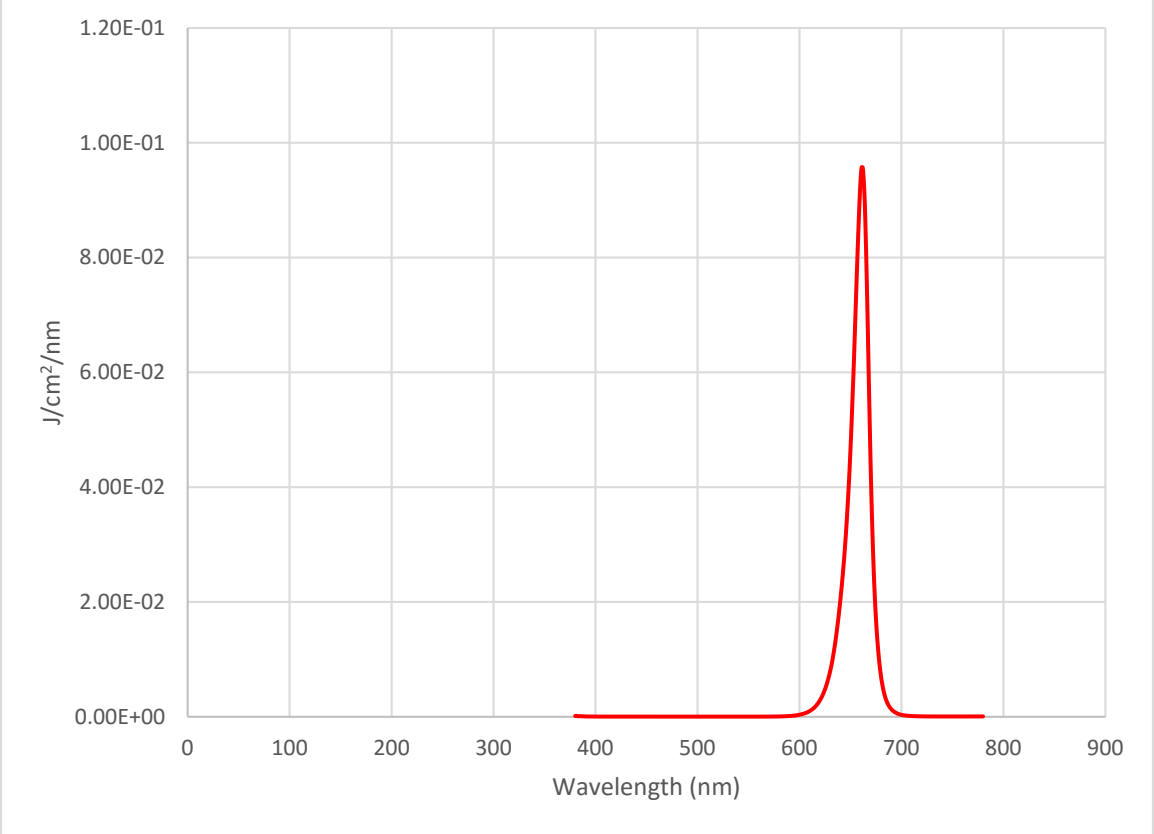

Figure 26. Lamp Intensity

MINUTES	J/CM²/NM
1	5.619322266
2	11.23864453
3	16.8579668
4	22.47728906
5	28.09661133
6	33.7159336
7	39.33525586
8	44.95457813
9	50.5739004
10	56.19322266

Table 7. Energy Output at 660 nm for 1-10 minutes

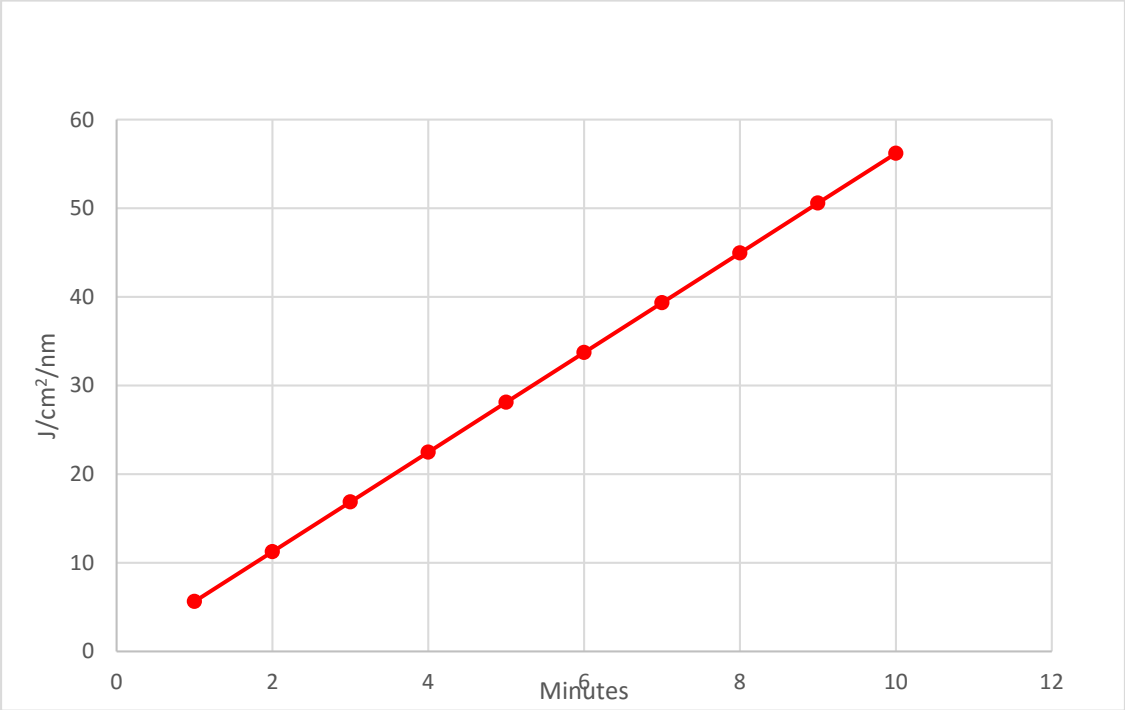

Figure 27. Energy output at 660 nm for 1-10 minutes

REFERENCES

Agostinis, P.; Berg, K.; Cengel, K. A.; Foster, T. H.; Girotti, A. W.; Gollnick, S. O.; Hahn, S. M.; Hamblin, M. R.; Juzeniene, A.; Kessel, D.; Korbelik, M.; Moan, J.; Mroz, P.; Nowis, D.; Piette, J.; Wilson, B. C.; Golab, J. Photodynamic therapy of cancer: An update. *CA: A Cancer Journal for Clinicians* **2011**, *61*, 250-281.

Ahmad, N.; Mukhtar, H. [32] Mechanism of photodynamic therapy-induced cell death. *Meth. Enzymol.* **2000**, *319*, 342-358.

American Cancer Society Information and Resources for Cancer: Breast, Colon, Prostate, Lung and Other FOrms. *http://www.cancer.org/* (accessed 3/29, 2016).

Amsterdam, A.; Nissen, R. M.; Sun, Z.; Swindell, E. C.; Farrington, S.; Hopkins, N. Identification of 315 genes essential for early zebrafish development. *Proc. Natl. Acad. Sci. U. S. A.* **2004**, *101*, 12792-12797.

Antony, A. C. Folate receptors. *Annu. Rev. Nutr.* **1996**, *16*, 501-521.

Aranda, A.; Pascual, A. Nuclear hormone receptors and gene expression. *Physiol. Rev.* **2001**, *81*, 1269-1304.

Azria, D.; Lemanski, C.; Zouhair, A.; Gutowski, M.; Belkacemi, Y.; Dubois, J. B.; Romieu, G.; Ozsahin, M. Adjuvant treatment of breast cancer by concomitant hormonotherapy and radiotherapy: state of the art. *Cancer Radiother.* **2004**, *8*, 188-196.

Bailey, L. B.; Gregory, J. F.,3rd Folate metabolism and requirements. *J. Nutr.* **1999**, *129*, 779-782.

Barnabé, A.; Aléssio, A. C. M.; Bittar, L. F.; de Moraes Mazetto, B.; Bicudo, A. M.; de Paula, E. V.; Höehr, N. F.; Annichino-Bizzacchi, J. M. Folate, Vitamin B12 and Homocysteine status in the post-folic acid fortification era in different subgroups of the Brazilian population attended to at a public health care center. *Nutrition journal* **2015**, *14*, 1.

Bechet, D.; Couleaud, P.; Frochot, C.; Viriot, M.; Guillemin, F.; Barberi-Heyob, M. Nanoparticles as vehicles for delivery of photodynamic therapy agents. *Trends Biotechnol.* **2008**, *26*, 612-621.

Bhatti, M.; Yahioglu, G.; Milgrom, L. R.; Garcia-Maya, M.; Chester, K. A.; Deonarain, M. P. Targeted photodynamic therapy with multiply-loaded recombinant antibody fragments. *International journal of cancer* **2008**, *122*, 1155-1163.

Biade, S.; Maziere, J.; Mora, L.; Santus, R.; Maziere, C.; Auclair, M.; Morliere, P.; Dubertret, L. Lovastatin potentiates the photocytotoxic effect of photofrin II delivered to HT29 human colonic adenocarcinoma cells by low density lipoprotein. *Photochem. Photobiol.* **1993**, *57*, 371-375.

Bisland, S. K.; Singh, D.; Gariépy, J. Potentiation of chlorin e6 photodynamic activity in vitro with peptide-based intracellular vehicles. *Bioconjug. Chem.* **1999**, *10*, 982-992.

Blair, J. E.; Shah, P.; Hedges, S. B. Evolutionary sequence analysis of complete eukaryote genomes. *BMC Bioinformatics* **2005**, *6*, 1.

Bonnett, R. Photodynamic Therapy in Historical Perspective. *Rev. Contemp. Pharmacother* **1999**, *10*, 1-17.

Bonnett, R. Photosensitizers of the porphyrin and phthalocyanine series for photodynamic therapy. *Chem. Soc. Rev.* **1995**, *24*, 19-33.

Botez, M. I.; Henry, R. E. *Folic acid in neurology, psychiatry, and internal medicine.* 1979; .

Botto, L. D.; Moore, C. A.; Khoury, M. J.; Erickson, J. D. Neural-tube defects. *N. Engl. J. Med.* **1999**, *341*, 1509-1519.

Briggs, J. P. The zebrafish: a new model organism for integrative physiology. *Am. J. Physiol. Regul. Integr. Comp. Physiol.* **2002**, *282*, R3-9.

Castano, A. P.; Demidova, T. N.; Hamblin, M. R. Mechanisms in photodynamic therapy: part one—photosensitizers, photochemistry and cellular localization. *Photodiagnosis and photodynamic therapy* **2004**, *1*, 279-293.

Chen, X.; Hui, L.; Foster, D. A.; Drain, C. M. Efficient synthesis and photodynamic activity of porphyrin-saccharide conjugates: targeting and incapacitating cancer cells. *Biochemistry (N. Y.)* **2004**, *43*, 10918-10929.

Choi, S. W.; Mason, J. B. Folate and carcinogenesis: an integrated scheme. *J. Nutr.* **2000**, *130*, 129-132.

Cieplik, F.; Tabenski, L.; Buchalla, W.; Maisch, T. Antimicrobial photodynamic therapy for inactivation of biofilms formed by oral key pathogens. *Front. Microbiol.* **2014**, *5*, 405.

Clarke, R.; Smith, A. D.; Jobst, K. A.; Refsum, H.; Sutton, L.; Ueland, P. M. Folate, vitamin B12, and serum total homocysteine levels in confirmed Alzheimer disease. *Arch. Neurol.* **1998**, *55*, 1449-1455.

Cowled, P.; Mackenzie, L.; Forbes, I. Potentiation of photodynamic therapy with haematoporphyrin derivatives by glucocorticoids. *Cancer Lett.* **1985**, *29*, 107-114.

de Vries, H. E.; Moor, A. C.; Dubbelman, T. M.; van Berkel, T. J.; Kuiper, J. Oxidized low-density lipoprotein as a delivery system for photosensitizers: implications for photodynamic therapy of atherosclerosis. *J. Pharmacol. Exp. Ther.* **1999**, *289*, 528-534.

Detty, M. R.; Gibson, S. L.; Wagner, S. J. Current clinical and preclinical photosensitizers for use in photodynamic therapy. *J. Med. Chem.* **2004**, *47*, 3897-3915.

Di Stasio, B.; Frochot, C.; Dumas, D.; Even, P.; Zwier, J.; Müller, A.; Didelon, J.; Guillemin, F.; Viriot, M.; Barberi-Heyob, M. The 2-aminoglucosamide motif improves cellular uptake and photodynamic activity of tetraphenylporphyrin. *Eur. J. Med. Chem.* **2005**, *40*, 1111-1122.

Dolmans, D.; E.J, G. J.; Dai, F.; Rakesh, J. Photodynamic Therapy for Cancer. *Nature Reviews* **2003**, *3*, 380-387.

Dougherty, T. J.; Gomer, C. J.; Henderson, B. W.; Jori, G.; Kessel, D.; Korbelik, M.; Moan, J.; Peng, Q. Photodynamic therapy. *J. Natl. Cancer Inst.* **1998**, *90*, 889-905.

Douillard, S.; Olivier, D.; Patrice, T. In vitro and in vivo evaluation of Radachlorin® sensitizer for photodynamic therapy. *Photochemical & Photobiological Sciences* **2009**, *8*, 405-413.

Eggener, S. E.; Coleman, J. A. Focal treatment of prostate cancer with vascular-targeted photodynamic therapy. *ScientificWorldJournal* **2008**, *8*, 963-973.

Ethirajan, M.; Chen, Y.; Joshia, P.; Pandey, R. K. The role of porphyrin chemistry in tumor imaging and photodynamic therapy. *Chem . Soc. Rev.* **2011**, *40*, 340-362.

Farias, N.; Ho, N.; Butler, S.; Delaney, L.; Morrison, J.; Shahrzad, S.; Coomber, B. L. The effects of folic acid on global DNA methylation and colonosphere formation in colon cancer cell lines. *J. Nutr. Biochem.* **2015**, *26*, 818-826.

Fernandez, J. M.; Bilgin, M. D.; Grossweiner, L. I. Singlet oxygen generation by photodynamic agents. *Journal of Photochemistry and Photobiology B: Biology* **1997**, *37*, 131-140.

Fleshker, S.; Preise, D.; Kalchenko, V.; Scherz, A.; Salomon, Y. Prompt Assessment of WST11-VTP Outcome Using Luciferase Transfected Tumors Enables Second Treatment and Increase in Overall Therapeutic Rate. *Photochem. Photobiol.* **2008**, *84*, 1231-1237.

Fodinger, M.; Horl, W. H.; Sunder-Plassmann, G. Molecular biology of 5,10-methylenetetrahydrofolate reductase. *J. Nephrol.* **2000**, *13*, 20-33.

Franck, B.; Nonn, A. Novel Porphyrinoids for Chemistry and Medicine by Biomimetic Syntheses. *Angew. Chem. Int. Ed. Engl.* **1995**, *34*, 1795-1811.

Frochot, C.; Di Stasio, B.; Barberi-Heyob, M.; Carre, M. C.; Zwier, J. M.; Guillemin, F.; Viriot, M. L. New glycosylated porphyrins for PDT applications. *Oftalmologia* **2003**, *56*, 62-66.

Fuchs, J.; Thiele, J. The role of oxygen in cutaneous photodynamic therapy. *Free Radical Biology and Medicine* **1998**, *24*, 835-847.

Gacio, A. F.; Fernandez-Marcos, C.; Swamy, N.; Dunn, D.; Ray, R. Photodynamic cell-kill analysis of breast tumor cells with a tamoxifen-pyropheophorbide conjugate. *J. Cell. Biochem.* **2006**, *99*, 665-670.

Giovannucci, E.; Stampfer, M. J.; Colditz, G. A.; Rimm, E. B.; Trichopoulos, D.; Rosner, B. A.; Speizer, F. E.; Willett, W. C. Folate, methionine, and alcohol intake and risk of colorectal adenoma. *J. Natl. Cancer Inst.* **1993**, *85*, 875-884.

Glickson, J. D.; Lund-Katz, S.; Zhou, R.; Choi, H.; Chen, I.; Li, H.; Corbin, I.; Popov, A. V.; Cao, W.; Song, L. Lipoprotein nanoplatform for targeted delivery of diagnostic and therapeutic agents. *Molecular imaging* **2008**, *7*, 101.

Golab, J.; Nowis, D.; Skrzycki, M.; Czeczot, H.; Baranczyk-Kuzma, A.; Wilczynski, G. M.; Makowski, M.; Mroz, P.; Kozar, K.; Kaminski, R.; Jalili, A.; Kopec', M.; Grzela, T.; Jakobisiak, M. Antitumor effects of photodynamic therapy are potentiated by 2-methoxyestradiol. A superoxide dismutase inhibitor. *J. Biol. Chem.* **2003**, *278*, 407-414.

Gomes, A. J.; Lunardi, C. N.; Tedesco, A. C. Characterization of biodegradable poly (D, L-lactide-co-glycolide) nanoparticles loaded with bacteriochlorophyll-a for photodynamic therapy. *Photomedicine and laser surgery* **2007**, *25*, 428-435.

Gomes, A. J.; Lunardi, L. O.; Marchetti, J. M.; Lunardi, C. N.; Tedesco, A. C. Photobiological and ultrastructural studies of nanoparticles of poly (lactic-co-glycolic acid)-containing bacteriochlorophyll-a as a photosensitizer useful for PDT treatment. *Drug Deliv.* **2005**, *12*, 159-164.

Gravier, J.; Schneider, R.; Frochot, C.; Bastogne, T.; Schmitt, F.; Didelon, J.; Guillemin, F.; Barberi-Heyob, M. Improvement of meta-tetra (hydroxyphenyl) chlorin-like photosensitizer selectivity with folate-based targeted delivery. Synthesis and in vivo delivery studies. *J. Med. Chem.* **2008**, *51*, 3867-3877.

Gross, J. M.; Dowling, J. E. Tbx2b is essential for neuronal differentiation along the dorsal/ventral axis of the zebrafish retina. *Proc. Natl. Acad. Sci. U. S. A.* **2005**, *102*, 4371-4376.

Hamblin, M. R.; Miller, J. L.; Ortel, B. Scavenger-Receptor Targeted Photodynamic Therapy. *Photochem. Photobiol.* **2000**, *72*, 533-540.

Han, S.; Kim, Y. Recent development of peptide coupling reagents in organic synthesis. *Tetrahedron* **2004**, *60*, 2447-2467.

Hedges, S. B.; Marin, J.; Suleski, M.; Paymer, M.; Kumar, S. Tree of life reveals clock-like speciation and diversification. *Mol. Biol. Evol.* **2015**, *32*, 835-845.

Hirth, A. U.; Michelsen, D. W. Photodynamische Tumortherapie. *Chem. Unserer Zeit* **1999**, *33*, 84-94.

Huang, B. X.; Kim, H.; Dass, C. Probing three-dimensional structure of bovine serum albumin by chemical cross-linking and mass spectrometry. *J. Am. Soc. Mass Spectrom.* **2004**, *15*, 1237-1247.

Isakau, H.; Parkhats, M.; Knyukshto, V.; Dzhagarov, B.; Petrov, E.; Petrov, P. Toward understanding the high PDT efficacy of chlorin e6–polyvinylpyrrolidone formulations: Photophysical and molecular aspects of photosensitizer–polymer interaction in vitro. *Journal of Photochemistry and Photobiology B: Biology* **2008**, *92*, 165-174.

James, D. A.; Swamy, N.; Paz, N.; Hanson, R. N.; Ray, R. Synthesis and estrogen receptor binding affinity of a porphyrin-estradiol conjugate for targeted photodynamic therapy of cancer. *Bioorg. Med. Chem. Lett.* **1999**, *9*, 2379-2384.

Jori, G. Far-red Absorbing photosensitizers; Their use in the Photodynamic Therapy of Tumors. *J. Photochem. Photobiol* **1992**, *62*, 371-378.

Josefen, L.; Boyle, R. Photodynamic therapy: novel third-generation photosensitizers one step closer? *British Journal of Pharmacology* **2008**, *154.1*, 1-3.

Kalli, K. R.; Oberg, A. L.; Keeney, G. L.; Christianson, T. J.; Low, P. S.; Knutson, K. L.; Hartmann, L. C. Folate receptor alpha as a tumor target in epithelial ovarian cancer. *Gynecol. Oncol.* **2008**, *108*, 619-626.

Kang, S.; Wong, P. W.; Norusis, M. Homocysteinemia due to folate deficiency. *Metab. Clin. Exp.* **1987**, *36*, 458-462.

Kao, T.; Chu, C.; Lee, G.; Hsiao, T.; Cheng, N.; Chang, N.; Chen, B.; Fu, T. Folate deficiency-induced oxidative stress contributes to neuropathy in young and aged zebrafish—implication in neural tube defects and Alzheimer's diseases. *Neurobiol. Dis.* **2014**, *71*, 234-244.

Kao, T. T.; Wang, K. C.; Chang, W. N.; Lin, C. Y.; Chen, B. H.; Wu, H. L.; Shi, G. Y.; Tsai, J. N.; Fu, T. F. Characterization and comparative studies of zebrafish and human recombinant dihydrofolate reductases--inhibition by folic acid and polyphenols. *Drug Metab. Dispos.* **2008**, *36*, 508-516.

Kelemen, L. E. The role of folate receptor α in cancer development, progression and treatment: cause, consequence or innocent bystander? *International journal of cancer* **2006**, *119*, 243-250.

Kimmel, C. B.; Ballard, W. W.; Kimmel, S. R.; Ullmann, B.; Schilling, T. F. Stages of embryonic development of the zebrafish. *Developmental dynamics* **1995**, *203*, 253-310.

Klotz, L.; Briviba, K.; Sies, H. Singlet oxygen mediates the activation of JNK by UVA radiation in human skin fibroblasts. *FEBS Lett.* **1997**, *408*, 289-291.

Kopelman, R.; Koo, Y. L.; Philbert, M.; Moffat, B. A.; Reddy, G. R.; McConville, P.; Hall, D. E.; Chenevert, T. L.; Bhojani, M. S.; Buck, S. M. Multifunctional nanoparticle platforms for in vivo MRI enhancement and photodynamic therapy of a rat brain cancer. *J Magn Magn Mater* **2005**, *293*, 404-410.

Kraljić, I.; Mohsni, S. E. A new method for the detection of singlet oxygen in aqueous solutions. *Photochem. Photobiol.* **1978**, *28*, 577-581.

Krishnaswamy, K.; Nair, K. M. Importance of folate in human nutrition. *Br. J. Nutr.* **2001**, *85*, S115-S124.

Laptev, R.; Nisnevitch, M.; Siboni, G.; Malik, Z.; Firer, M. Intracellular chemiluminescence activates targeted photodynamic destruction of leukaemic cells. *Br. J. Cancer* **2006**, *95*, 189-196.

Leamon, C. P.; Low, P. Cytotoxicity of momordin-folate conjugates in cultured human cells. *J. Biol. Chem.* **1992**, *267*, 24966-24971.

Leamon, C. P.; Pastan, I.; Low, P. Cytotoxicity of folate-Pseudomonas exotoxin conjugates toward tumor cells. Contribution of translocation domain. *J. Biol. Chem.* **1993**, *268*, 24847-24854.

Leamon, C. P.; Reddy, J. A. Folate-targeted chemotherapy. *Adv. Drug Deliv. Rev.* **2004**, *56*, 1127-1141.

Lee, M. S.; Bonner, J. R.; Bernard, D. J.; Sanchez, E. L.; Sause, E. T.; Prentice, R. R.; Burgess, S. M.; Brody, L. C. Disruption of the folate pathway in zebrafish causes developmental defects. *BMC developmental biology* **2012**, *12*, 1.

Lemire, R. J. Neural tube defects. *JAMA* **1988**, *259*, 558-562.

Lu, Y.; Low, P. S. Folate-mediated delivery of macromolecular anticancer therapeutic agents. *Adv. Drug Deliv. Rev.* **2012**, *64*, 342-352.

Luo, W.; Liu, R.; Zhu, J.; Li, Y.; Liu, H. Subcellular location and photodynamic therapeutic effect of chlorin e6 in the human tongue squamous cell cancer Tca8113 cell line. *Oncology letters* **2015**, *9*, 551-556.

Ma, Y.; Wu, M.; Li, D.; Li, X.; Li, P.; Zhao, J.; Luo, M.; Guo, C.; Gao, X.; Lu, C. Embryonic developmental toxicity of selenite in zebrafish (Danio rerio) and prevention with folic acid. *Food and chemical toxicology* **2012**, *50*, 2854-2863.

Malatesti, N.; Smith, K.; Savoie, H.; Greenman, J.; Boyle, R. W. Synthesis and in vitro investigation of cationic 5, 15-diphenyl porphyrin-monoclonal antibody conjugates as targeted photodynamic sensitisers. *Int. J. Oncol.* **2006**, *28*, 1561-1569.

Martins, J.; Madeira, V. t.; Almeida, L.; Laranjinha, J. Photoactivation of phthalocyanine-loaded low density lipoproteins induces a local oxidative stress that propagates to human erythrocytes: protection by caffeic acid. *Free Radic. Res.* **2002**, *36*, 319-328.

Mayo, G. L.; Melendez, R. F.; Kumar, N.; McKinnon, S. J.; Glickman, R. D. Antibody-targeted photodynamic therapy. *Am. J. Ophthalmol.* **2003**, *136*, 1151-1152.

McCarthy, J. R.; Perez, J. M.; Brückner, C.; Weissleder, R. Polymeric nanoparticle preparation that eradicates tumors. *Nano letters* **2005**, *5*, 2552-2556.

Meenan, J.; O'Hallinan, E.; Scott, J.; Weir, D. G. Epithelial cell folate depletion occurs in neoplastic but not adjacent normal colon mucosa. *Gastroenterology* **1997**, *112*, 1163-1168.

Mew, D.; Wat, C.; Towers, G.; Levy, J. Photoimmunotherapy: treatment of animal tumors with tumor-specific monoclonal antibody-hematoporphyrin conjugates. *The Journal of Immunology* **1983**, *130*, 1473-1477.

Mills, J. L.; Lee, Y.; Conley, M.; Kirke, P.; McPartlin, J.; Weir, D. G.; Scott, J. M. Homocysteine metabolism in pregnancies complicated by neural-tube defects. *The Lancet* **1995**, *345*, 149-151.

Mojzisova, H.; Bonneau, S.; Vever-Bizet, C.; Brault, D. The pH-dependent distribution of the photosensitizer chlorin e6 among plasma proteins and membranes: a physico-chemical approach. *Biochimica et Biophysica Acta (BBA)-Biomembranes* **2007**, *1768*, 366-374.

Montalbetti, C. A.; Falque, V. Amide bond formation and peptide coupling. *Tetrahedron* **2005**, *61*, 10827-10852.

Mosinger, J.; Mička, Z. Quantum yields of singlet oxygen of metal complexes of meso-tetrakis (sulphonatophenyl) porphine. *J. Photochem. Photobiol. A.* **1997**, *107*, 77-82.

Mroz, P.; Yaroslavsky, A.; Kharkwa, G. B.; Hamblin, M. R. Cell Death Pathways in Photodynamic Therapy of Cancer. *Cancers* **2011**, *3 (2)*, 2516-2539.

Müller-Breitkreutz, K.; Mohr, H.; Briviba, K.; Sies, H. Inactivation of viruses by chemically and photochemically generated singlet molecular oxygen. *Journal of photochemistry and photobiology B: Biology* **1995**, *30*, 63-70.

Muralidharan, P.; Sarmah, S.; Marrs, J. A. Zebrafish retinal defects induced by ethanol exposure are rescued by retinoic acid and folic acid supplement. *Alcohol* **2015**, *49*, 149-163.

National Cancer Institute Comprehensive Cancer Information. *www.cancer.gov* (accessed 3/29, 2016).

Nelson, J. S.; Roberts, W. G.; Berns, M. W. In vivo studies on the utilization of mono-L-aspartyl chlorin (NPe6) for photodynamic therapy. *Cancer Res.* **1987**, *47*, 4681-4685.

Nyman, E. S.; Hynninen, P. H. Research advances in the use of tetrapyrrolic photosensitizers for photodynamic therapy. *Journal of Photochemistry and Photobiology B: Biology* **2004**, *73*, 1-28.

Orenstein, A.; Kostenich, G.; Roitman, L.; Shechtman, Y.; Kopolovic, Y.; Ehrenberg, B.; Malik, Z. A comparative study of tissue distribution and photodynamic therapy selectivity of chlorin e6, Photofrin II and ALA-induced protoporphyrin IX in a coloncarcinoma model. *Br. J. Cancer* **1996**, *73 (8)*, 937-944.

Oseroff, A. R.; Ohuoha, D.; Hasan, T.; Bommer, J. C.; Yarmush, M. L. Antibody-targeted photolysis: selective photodestruction of human T-cell leukemia cells using monoclonal antibody-chlorin e6 conjugates. *Proceedings of the National Academy of Sciences* **1986**, *83*, 8744-8748.

Pan, X.; Lee, R. J. Tumour-selective drug delivery via folate receptor-targeted liposomes. *Expert opinion on drug delivery* **2004**, *1*, 7-17.

Pandey, R. K.; Zheng, G., Eds.; In *The Porphyrin Handbook;* Kadish, K. M., Smith, K. M. and Guilard, R., Eds.; 2000; Vol. 6, pp 157-230.

Parker, N.; Turk, M. J.; Westrick, E.; Lewis, J. D.; Low, P. S.; Leamon, C. P. Folate receptor expression in carcinomas and normal tissues determined by a quantitative radioligand binding assay. *Anal. Biochem.* **2005**, *338*, 284-293.

Parkin, C. A.; Allen, C. E.; Ingham, P. W. Hedgehog signalling is required for cloacal development in the zebrafish embryo. *Int. J. Dev. Biol.* **2009**, *53*, 45.

Pervaiz, S.; Malini, O. Art and Science of Photodynamic Therapy. *Clinical and Experimental Pharmacology and Physiology* **2006**, *33*, 551-556.

Polo, L.; Valduga, G.; Jori, G.; Reddi, E. Low-density lipoprotein receptors in the uptake of tumour photosensitizers by human and rat transformed fibroblasts. *Int. J. Biochem. Cell Biol.* **2002**, *34*, 10-23.

Preise, D.; Oren, R.; Glinert, I.; Kalchenko, V.; Jung, S.; Scherz, A.; Salomon, Y. Systemic antitumor protection by vascular-targeted photodynamic therapy involves cellular and humoral immunity. *Cancer Immunology, Immunotherapy* **2009**, *58*, 71-84.

Pyati, U. J.; Cooper, M. S.; Davidson, A. J.; Nechiporuk, A.; Kimelman, D. Sustained Bmp signaling is essential for cloaca development in zebrafish. *Development* **2006**, *133*, 2275-2284.

Qian, P.; Evensen, J. F.; Rimington, C.; Moan, J. A comparison of different photosensitizing dyes with respect to uptake C3H-tumors and tissues of mice. *Cancer Lett.* **1987**, *36*, 1-10.

Reddi, E. Role of delivery vehicles for photosensitizers in the photodynamic therapy of tumours. *Journal of Photochemistry and Photobiology B: Biology* **1997**, *37*, 189-195.

Reynolds, E. Folic acid, ageing, depression, and dementia. *Br. Med. J.* **2002**, *324*, 1512.

Ricci-Júnior, E.; Marchetti, J. M. Zinc (II) phthalocyanine loaded PLGA nanoparticles for photodynamic therapy use. *Int. J. Pharm.* **2006**, *310*, 187-195.

Robertson, C. A.; Hawkins, E.; Abrahamse, H. Photodynamic Therapy (PDT): A Short Review on Cellular Mechanisms and Cancer Research Applications for PDT. *Journal of Photochemistry and Photobiology B: Biology* **2009**, *96*, 1-8.

Rosenquist, T. H.; Ratashak, S. A.; Selhub, J. Homocysteine induces congenital defects of the heart and neural tube: effect of folic acid. *Proc. Natl. Acad. Sci. U. S. A.* **1996**, *93*, 15227-15232.

Ross, B.; Rehemtulla, A.; Koo, Y. L.; Reddy, R.; Kim, G.; Behrend, C.; Buck, S.; Schneider, R. J.; Philbert, M. A.; Weissleder, R. In *In Photonic and magnetic nanoexplorers for biomedical use: from subcellular imaging to cancer diagnostics and therapy;* Biomedical Optics 2004; International Society for Optics and Photonics: 2004; , pp 76-83.

Seery, M. Photodynamic Therapy: An Overview . *https://photochemistry.wordpress.com/2012/12/16/photodynamic-therapy-an-overview/* (accessed 1/20, 2016).

Seshadri, S. Prevalence of micronutrient deficiency particularly of iron, zinc and folic acid in pregnant women in South East Asia. *Br. J. Nutr.* **2001**, *85*, S87-S92.

Sharman, W. M.; van Lier, J. E.; Allen, C. M. Targeted photodynamic therapy via receptor mediated delivery systems. *Adv. Drug Deliv. Rev.* **2004**, *56*, 53-76.

Shen, X.; Liang, D.; Zhang, P. The development of three long universal nuclear protein-coding locus markers and their application to osteichthyan phylogenetics with nested PCR. *PloS one* **2012**, *7*, e39256.

Silverstein, S. C.; Steinman, R. M.; Cohn, Z. A. Endocytosis. *Annu. Rev. Biochem.* **1977**, *46*, 669-722.

Sokolov, V. V.; Stranadko, E. F.; Zharkova, N. N. The Photodynamic Therapy of Malignant Tumors in Basic Sites with the Preparations Photchem and Photsens (the results of 3 years of observations). *Vopr. Onkol.* **1995**, *41*, 134-138.

Song, L. Naphthalocyanine-reconstituted LDL nanoparticles for in vivo cancer imaging and treatment. *International Journal of Nanomedicine* **2007**, *2*, 767-774.

Soukos, N. S.; Ximenez-Fyvie, L. A.; Hamblin, M. R.; Socransky, S. S.; Hasan, T. Targeted antimicrobial photochemotherapy. *Antimicrob. Agents Chemother.* **1998**, *42*, 2595-2601.

Spenlehauer, G.; Vert, M.; Benoit, J.; Boddaert, A. In vitro and in vivo degradation of poly (D, L lactide/glycolide) type microspheres made by solvent evaporation method. *Biomaterials* **1989**, *10*, 557-563.

Sudimack, J.; Lee, R. J. Targeted drug delivery via the folate receptor. *Adv. Drug Deliv. Rev.* **2000**, *41*, 147-162.

Sun, S.; Gui, Y.; Jiang, Q.; Song, H. Dihydrofolate reductase is required for the development of heart and outflow tract in zebrafish. *Acta Biochim. Biophys. Sin. (Shanghai)* **2011**, *43*, 957-969.

Sun, S.; Gui, Y.; Wang, Y.; Qian, L.; Liu, X.; Jiang, Q.; Song, H. Effects of methotrexate on the developments of heart and vessel in zebrafish. *Acta Biochim. Biophys. Sin. (Shanghai)* **2009**, *41*, 86-96.

Sutton, J.; Clarke, O.; Fernandez, N.; Boyle, R. Porphyrin, chlorin, and bacteriochlorin isothiocyanates: useful reagents for the synthesis of photoactive bioconjugates. *Bioconjug. Chem.* **2002**, *13*, 249-263.

Swamy, N.; James, D. A.; Mohr, S. C.; Hanson, R. N.; Ray, R. An estradiol-porphyrin conjugate selectively localizes into estrogen receptor-positive breast cancer cells. *Bioorg. Med. Chem.* **2002**, *10*, 3237-3243.

Swamy, N.; Purohit, A.; Fernandez-Gacio, A.; Jones, G. B.; Ray, R. Nuclear estrogen receptor targeted photodynamic therapy: Selective uptake and killing of MCF-7 breast cancer cells by a C17α-alkynylestradiol-porphyrin conjugate. *J. Cell. Biochem.* **2006**, *99*, 966-977.

Taquet, J.; Frochot, C.; Manneville, V.; Barberi-Heyob, M. Phthalocyanines covalently bound to biomolecules for a targeted photodynamic therapy. *Curr. Med. Chem.* **2007**, *14*, 1673-1687.

Trachtenberg, J.; Weersink, R. A.; Davidson, S. R.; Haider, M. A.; Bogaards, A.; Gertner, M. R.; Evans, A.; Scherz, A.; Savard, J.; Chin, J. L. Vascular-targeted photodynamic therapy (padoporfin, WST09) for recurrent prostate cancer after failure of external beam radiotherapy: a study of escalating light doses. *BJU Int.* **2008**, *102*, 556-562.

Urizzi, P.; Allen, C. M.; Langlois, R.; Ouellet, R.; La Madeleine, C.; Van Lier, J. E. Low-density lipoprotein-bound aluminum sulfophthalocyanine: targeting tumor cells for photodynamic therapy. *Journal of Porphyrins and Phthalocyanines* **2001**, *5*, 154-160.

Uspenskii, L. V.; Chistov, L. V.; Kogan, E. A.; Loshchenov, V. B.; Ablitsov, I.; Rybin, V. K.; Zavodnov, V. I.; Shiktorov, D. I.; Serbinenko, N. F.; Semenova, I. G. Endobronchial laser therapy in complex preoperative preparation of patients with lung diseases. *Khirurgiia (Mosk)* **2000**, *(2)*, 38-40.

Vrouenraets, M.; Visser, G.; Snow, G.; van Dongen, G. Basic principles, applications in oncology and improved selectivity of photodynamic therapy**.**. *Anticancer Res* **2003**, *23 (1B)*, 505-522.

Wala; Sheldon Prevention of neural tube defects: results of the Medical Research Council Vitamin Study. *MRC Vitamin Study Research Group;* **1991**, *338*, 131-137.

Wald, N. J.; Watt, H. C.; Law, M. R.; Weir, D. G.; McPartlin, J.; Scott, J. M. Homocysteine and ischemic heart disease: results of a prospective study with implications regarding prevention. *Arch. Intern. Med.* **1998**, *158*, 862-867.

Wawrzyńska, M.; Kałas, W.; Biały, D.; Zioło, E.; Arkowski, J.; Mazurek, W.; Strządała, L. In vitro photodynamic therapy with chlorin e6 leads to apoptosis of human vascular smooth muscle cells. *Arch. Immunol. Ther. Exp. (Warsz.)* **2010**, *58*, 67-75.

Willett, W. C. Micronutrients and cancer risk. *Am. J. Clin. Nutr.* **1994**, *59*, 1162S-1165S.

Williams, J.; Mai, C. T.; Mulinare, J.; Isenburg, J.; Flood, T. J.; Ethen, M.; Frohnert, B.; Kirby, R. S. Updated estimates of neural tube defects prevented by mandatory folic Acid fortification-United States, 1995–2011. *MMWR Morb. Mortal. Wkly. Rep.* **2015**, *64*, 1-5.

Woodburn, K.; Vardaxis, N.; Hill, J.; Kaye, A.; Phillips, D. Subcellular localization of porphyrins using confocal laser scanning microscopy. *Photochem. Photobiol.* **1991**, *54*, 725-732.

Woooburn, K.; Vardaxis, N.; Hill, J.; Kaye, A.; Reiss, J.; Phillips, D. Evaluation of porphyrin characteristics required for photodynamic therapy. *Photochem. Photobiol.* **1992**, *55*, 697-704.

World Health Organization Cancer. *http://www.who.int/cancer/en/* (accessed 3/29, 2016).

Yamamoto, T.; Furukawa, K.; Hiyoshi, T.; Konaka, C.; Kato, H. Photodynamic Therapy for Cancers. *Curr. Sci.* **1999**, *77*, 894-903.

Yoo, H. S.; Park, T. G. Folate-receptor-targeted delivery of doxorubicin nano-aggregates stabilized by doxorubicin–PEG–folate conjugate. *J. Controlled Release* **2004**, *100*, 247-256.

Zeisser-Labouèbe, M.; Lange, N.; Gurny, R.; Delie, F. Hypericin-loaded nanoparticles for the photodynamic treatment of ovarian cancer. *Int. J. Pharm.* **2006**, *326*, 174-181.

Zhang, D.; Wu, M.; Zeng, Y.; Wu, L.; Wang, Q.; Han, X.; Liu, X.; Liu, J. Chlorin e6 conjugated poly (dopamine) nanospheres as PDT/PTT dual-modal therapeutic agents for enhanced cancer therapy. *ACS applied materials & interfaces* **2015**, *7*, 8176-8187.

Zhao, X.; Li, H.; Lee, R. J. Targeted drug delivery via folate receptors. *Expert opinion on drug delivery* **2008**, *5*, 309-319.

Zhao, R.; Diop-Bove, N.; Visentin, M.; Goldman, I. D. Mechanisms of membrane transport of folates into cells and across epithelia. *Annu. Rev. Nutr.* **2011**, *31*, 177-201.

Zheng, G.; Graham, A.; Shibata, M.; Missert, J. R.; Oseroff, A. R.; Dougherty, T. J.; Pandey, R. K. Synthesis of β-galactose-conjugated chlorins derived by enyne metathesis as galectin-specific photosensitizers for photodynamic therapy. *J. Org. Chem.* **2001**, *66*, 8709-8716.

Zheng, G.; Chen, J.; Li, H.; Glickson, J. D. Rerouting lipoprotein nanoparticles to selected alternate receptors for the targeted delivery of cancer diagnostic and therapeutic agents. *Proc. Natl. Acad. Sci. U. S. A.* **2005**, *102*, 17757-17762.

Zwicke, G. L.; Mansoori, G. A.; Jeffery, C. J. Utilizing the folate receptor for active targeting of cancer nanotherapeutics. *Nano reviews* **2012**, *3*.

VITA

RoJenia N. Jones attended Thornton Fractional South High School in Lansing, IL from 1999-2003. She received her B.S. in Chemistry and African/African-American Studies from Dominican University in River Forest, IL in 2007. She received her M.S. in Chemistry from Ball State University in Muncie, IN where she was awarded Graduate Researcher of the Year in 2009.